HHS Public Access

Author manuscript

Cell Rep. Author manuscript; available in PMC 2023 September 27.

Published in final edited form as:

Cell Rep. 2023 July 25; 42(7): 112807. doi:10.1016/j.celrep.2023.112807.

Activation of autophagy depends on Atg1/Ulk1-mediated phosphorylation and inhibition of the Hsp90 chaperone machinery

Sarah J. Backe[1,2], **Rebecca A. Sager**[1,2], **Jennifer A. Heritz**[1,2,3], **Laura A. Wengert**[1,3], **Katherine A. Meluni**[1,2], **Xavier Aran-Guiu**[4], **Barry Panaretou**[5], **Mark R. Woodford**[1,2,3], **Chrisostomos Prodromou**[6], **Dimitra Bourboulia**[1,2,3], **Mehdi Mollapour**[1,2,3,7,8,*]

[1]Department of Urology, SUNY Upstate Medical University, Syracuse, NY 13210, USA

[2]Upstate Cancer Center, SUNY Upstate Medical University, Syracuse, NY 13210, USA

[3]Department of Biochemistry and Molecular Biology, SUNY Upstate Medical University, Syracuse, NY 13210, USA

[4]Biochemistry and Biomedicine, School of Life Sciences, University of Sussex, Brighton, UK

[5]School of Cancer and Pharmaceutical Sciences, Institute of Pharmaceutical Science, King's College London, London SE1 9NQ, UK

[6]Genome Damage and Stability Centre, University of Sussex, Brighton BN1 9RQ, UK

[7]Twitter: @medmol

[8]Lead contact

SUMMARY

Cellular homeostasis relies on both the chaperoning of proteins and the intracellular degradation system that delivers cytoplasmic constituents to the lysosome, a process known as autophagy. The crosstalk between these processes and their underlying regulatory mechanisms is poorly understood. Here, we show that the molecular chaperone heat shock protein 90 (Hsp90) forms a complex with the autophagy-initiating kinase Atg1 (yeast)/Ulk1 (mammalian), which suppresses its kinase activity. Conversely, environmental cues lead to Atg1/Ulk1-mediated phosphorylation of a conserved serine in the amino domain of Hsp90, inhibiting its ATPase activity and altering

*Correspondence: mollapom@upstate.edu.

AUTHOR CONTRIBUTIONS

Conceptualization of the project, M.M.; experimental design, investigation, data analysis, and presentation, S.J.B., R.A.S., J.A.H., L.A.W., K.A.M., X.A.-G., B.P., M.R.W., C.P., D.B., and M.M.; original draft, S.J.B. and M.M.; contributions to manuscript writing, review, and editing, S.J.B., R.A.S., B.P., M.R.W., C.P., D.B., and M.M.; supervision, M.M. All authors read the manuscript and provided their final approval for the content.

SUPPLEMENTAL INFORMATION

Supplemental information can be found online at https://doi.org/10.1016/j.celrep.2023.112807.

DECLARATION OF INTERESTS

The authors declare no competing interests.

INCLUSION AND DIVERSITY

We support inclusive, diverse, and equitable conduct of research.

the chaperone dynamics. These events impact a conformotypic peptide adjacent to the activation and catalytic loop of Atg1/Ulk1. Finally, Atg1/Ulk1-mediated phosphorylation of Hsp90 leads to dissociation of the Hsp90:Atg1/Ulk1 complex and activation of Atg1/Ulk1, which is essential for initiation of autophagy. Our work indicates a reciprocal regulatory mechanism between the chaperone Hsp90 and the autophagy kinase Atg1/Ulk1 and consequent maintenance of cellular proteostasis.

In brief

Backe et al. show a reciprocal regulatory mechanism between the chaperone Hsp90 and the autophagy kinase client Atg1/Ulk1. This consequently leads to maintenance of cellular proteostasis and activation of autophagy.

Graphical Abstract

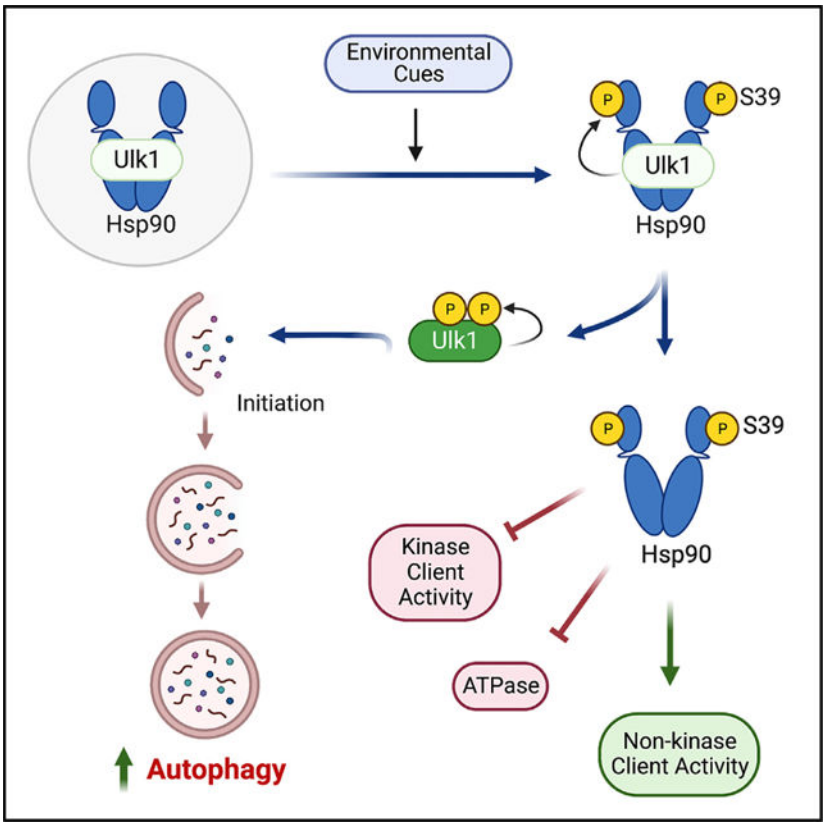

INTRODUCTION

The molecular chaperone heat shock protein 90 (Hsp90) is involved in maintaining the stability and activity of a large and diverse group of proteins commonly referred to as client proteins.[1] The vast majority of Hsp90 clients (https://www.picard.ch/downloads/Hsp90interactors.pdf) are protein kinases, and many are also involved in phosphorylation and regulation of the Hsp90 chaperone function.[2,3] Additionally, some of these Hsp90

phosphorylation events feedback to control the specific signaling and cellular process associated with that particular kinase.[3–6]

Hsp90 chaperone function is coupled to its ATPase activity, which is regulated by co-chaperones as well as post-translational modifications (PTMs), which, collectively, is known as the "chaperone code."[3,7–9] Hsp90 exists as a homodimer, and each protomer is comprised of three structural domains.[10,11] The amino-terminal domain contains the nucleotide-binding pocket,[12,13] which is also a binding site for Hsp90 inhibitors.[14,15] The middle domain serves as the binding site for the majority of client proteins and many co-chaperones.[1,8] The amino and middle domains are connected by a flexible and highly charged linker region.[16,17] The carboxyl domain is constitutively dimerized[18–21] and contains the extreme C-terminal MEEVD sequence that serves as an interaction site for tetratricopeptide repeat (TPR)-domain-containing co-chaperones.[22–25] Upon ATP binding to the nucleotide binding pocket, Hsp90 undergoes conformational changes, eventual transient dimerization of the amino-terminal domain, and subsequent ATP hydrolysis.[26–29] This provides a platform for binding and release and chaperoning of the client proteins.

Autophagy is a lysosomal-dependent cellular pathway that mediates the degradation of organelles, protein aggregates, and specific proteins and is essential for cell survival, development, and homeostasis.[30,31] There are three main pathways where different cargos are delivered to lysosomes. They include macroautophagy, microautophagy, and chaperone-mediated autophagy.[31–33] In the latter process, the cargo is selectively recognized by a chaperone protein and then internalized into a lysosome for its degradation.[34]

In this study, we dissected the relationship between macroautophagy (hereafter autophagy) and the molecular chaperone Hsp90. Hsp90 is subject to an array of PTMs that regulate its chaperone function.[3,35] The Atg1 (yeast)/Ulk1 (mammalian) kinase is one of the most upstream components of the autophagy machinery and is also an Hsp90 client protein.[34,36] Here, we showed that Hsp90 binds to and forms a complex with Atg1/Ulk1, which suppresses its kinase activity. Activation of Atg1/Ulk1, however, causes it to phosphorylate Hsp90, inhibiting Hsp90 ATPase activity and altering the chaperone dynamics. These events lead to dissociation of the Hsp90:Atg1/Ulk1 complex and activation of Atg1/Ulk1, which is essential for the initiation of autophagy.

RESULTS

Autophagy-initiating kinase Atg1/Ulk1 phosphorylates a conserved serine in the amino domain of Hsp90

Phosphorylation motifs, or consensus amino acid sequences, can aid in the understanding of kinase-substrate interactions to provide deeper comprehension of the regulation that governs cellular pathways. The commercially available phosphorylated (phospho)-(Ser/Thr) Phe antibody (Cell Signaling Technology) detects phosphoserine or threonine in the context of tyrosine, tryptophan, or phenylalanine at the −1 position or phenylalanine at the +1 position (Figure 1A). We identified five potential phosphorylation sites that fit the consensus motif Y/W/F-phospho-(p)S/T or pS/T-F: two threonine residues (T5, T157) and three serine residues (S25, S126, S155) in the amino domain of yeast Hsp82 (yHsp90) (Figure

1A). We took advantage of our previously published yHsp90-PreScission construct in which a PreScission Protease cleavage site was introduced between the amino domain and the adjacent charged linker region[37,38] (Figure 1A). This allowed us to separate the amino domain from the full-length yHsp90 protein. These yHsp90 proteins were His_6 epitope tagged at the amino terminus and expressed as the sole copy of Hsp90 in yeast. We expressed and isolated these yHsp90 phosphomutants by Ni-NTA agarose pull-down followed by treatment with PreScission Protease to isolate the yHsp90 amino domain. Immunoblotting of the isolated amino domains with antibodies to both hexahistidine and p-(Ser/Thr) Phe antibodies showed that S25 is subject to phosphorylation (Figure 1B). We further showed that the p-(Ser/Thr) Phe antibody is unable to detect the full-length non-phospho S25A-yHsp90 mutant, suggesting this is the only site within the full-length protein that fits this motif (Figure S1A). These data allowed us to screen the yeast non-essential kinase deletion strain collection and identify Atg1 as the kinase targeting yHsp90-S25 (Figures S1B and S1C; Table S1). Using pan-phospho-serine and p-(Ser/Thr) Phe antibodies with the full-length wild-type yHsp90 (WT-yHsp90) and the S25A mutant, we provided definitive data that Atg1 only phosphorylates yHsp90-S25 (Figure 1C). Serine 25 is highly conserved in eukaryotic Hsp90 proteins, and S39 is the equivalent residue in human Hsp90α (hHsp90α). To assess whether hHsp90α-S39 is also subject to phosphorylation by Atg1/Ulk1, we utilized DLD-1 (colorectal adenocarcinoma) cell lines that either express two copies of *ULK1*-WT (*WT/WT*) or have *ULK1* knocked out and a kinase-dead *ULK1*-K46I mutant reintroduced on a single allele (*KO/K46I*). Using anti-p-(Ser/Thr) Phe antibody, we showed hHsp90α-WT phosphorylation in *ULK1-WT/WT* DLD-1 cells. Notably, we did not detect phosphorylation of non-phosphomutant hHsp90α-S39A (Figure 1D). We were also unable to observe hHsp90α phosphorylation with the same antibody in the DLD-1 cells expressing only kinase-dead *ULK1*-K46I (Figure 1D). Next, we used bacterially expressed and purified hHsp90α-His_6 and S39A together with recombinant Ulk1 (Abcam) in an *in vitro* kinase assay. Our data provided further evidence toward Ulk1-mediated phosphorylation of hHsp90α-S39 since we were unable to detect the phosphorylation of hHsp90α-S39A with p-(Ser/Thr) Phe antibody (Figure 1E).

Contrary to previously published work,[39] we were unable to confirm Ulk1-mediated phosphorylation of the co-chaperone Cdc37 (Figures S1D and S1E). We were only able to confirm the phosphorylation of S13 and S125 in Cdc37, but these were not catalyzed by Ulk1 (Figure S1D). Taken together, our data showed Atg1/Ulk1 phosphorylates a conserved serine site (yS25/hS39) in the amino domain of Hsp90.

Atg1/Ulk1 phosphorylation of Hsp90 reduces its ATPase activity and impacts co-chaperone binding

In order to determine the effect of S25 phosphorylation on Hsp90 function, we first examined the ATPase activity of the yeast Hsp90 phosphomutants. The non-phosphorylatable S25A and phosphomimetic S25E as well as WT yHsp90 were expressed and purified from bacteria, and their ATPase activity was measured using a coupled enzyme assay.[40] We found that the S25A mutation led to a decrease in yHsp90 ATPase activity (~60%) compared with the WT yHsp90 (Figure 2A). The phosphomimetic S25E mutation led to a further decrease in ATPase activity to ~25% of WT (Figure 2A). We next examined

the binding affinity of the ATP analog AMPPNP with S25A and S25E compared with WT yHsp90 using isothermal titration calorimetry (ITC) (Figure 2B). We found a slight decrease in the affinity of binding of AMPPNP to S25A and S25E. Notably, when we expressed hHsp90α-FLAG-WT, S39A, and S39E in mammalian cells, we did not observe changes in binding to ATP or a biotinylated Hsp90 inhibitor (biotin-ganetespib [Biotin-GB]) (Figures S2A–S2C).

The co-chaperone Aha1 is the potent activator of Hsp90 ATPase activity.[41–44] We therefore measured the binding affinity of the recombinant yeast Aha1 (yAha1) with the phosphomutants. Both S25 phosphomutants bound Aha1 with similar affinity to WT yHsp90 (Figure 2B). We next pulled down yHsp90 and the S25A and S25E mutants from yeast using Ni-NTA and confirmed the similar affinity of yAha1 to S25A and S25E (Figures 2C and 2D). Interestingly, the binding of Sti1 was diminished by S25E mutation (Figures 2C and 2D). Conversely, interaction with Cdc37 and Sba1 were both increased in the S25E mutant (Figures 2C and 2D). We next expressed hHsp90α-FLAG and the S39A and S39E mutants in HEK293 cells and found a similar binding pattern to the co-chaperones Aha1, HOP, Cdc37, and p23 (Figures 2D and 2E). Taken together, our data suggest that phosphomutants of S25 negatively impact yHsp90 ATP binding and ATPase activity. Additionally, the binding of these yHsp90 and hHsp90α phosphomutants to the Hsp90 “late complex” co-chaperones, p23 and Cdc37, was increased. Collectively, our data suggest that Hsp90 phosphomutants impact the chaperone function.

Hsp90 phosphorylation and activation of autophagy differentially regulate client proteins

In order to further characterize the chaperone function of the S25 phosphomutants, we examined the stability and activity of a well-established kinase client, v-Src. We were able to express v-Src under the *GAL1* promoter in yeast expressing either WT yHsp90 or the S25A or S25E mutants. Although the stability and activity (evident by pan-phosphotyrosine antibody) of v-Src in S25A-expressing yeast was greater than WT, v-Src was completely unstable in yeast expressing the S25E mutant (Figure 3A). We obtained similar data for the stability of a native yeast Hsp90 client, active Ste11 kinase (Ste11ΔN), the ortholog of mammalian Raf-1 (Figure 3B).[45,46] The MAPK kinase Mpk1/ Slt2 (an Erk5 ortholog) is an Hsp90 client and is involved in maintaining the cell wall integrity pathway.[47] We activated Slt2 by treating the yeast cells with 10 mM caffeine and measured the activity of Slt2 using the RLM1-*lacZ* reporter. Similar to the other kinase clients v-Src and Ste11, Slt2 activity was significantly increased in the S25A cells even in the absence of stress but can be further increased with caffeine stress (Figures 3C and S3A).

In order to obtain insight into the impact of the S25 phosphomutants on chaperoning of non-kinase clients, we first examined Hsf1 activity using an *HSE-lacZ* promoter assay. Our data showed that phosphomimetic S25E caused an increase in heat shock response even in the absence of heat stress (Figures 3D and S3B). We obtained similar data with the activity of the steroid hormone receptors (SHRs) glucocorticoid receptor (GR), androgen receptor (AR), and estrogen receptor α (ERα) following hormone stimulation (Figures 3E–3G and S3C–S3E).[48–50] Collectively, these data suggest that phosphomimetic S25E has a negative impact on the stability and activity of the kinase clients v-Src, Ste11, and Slt2. Conversely,

this phosphomimetic mutant has the opposite effect and positively impacted the activity of Hsf1 and the SHR non-kinase clients.

Phosphorylation of Hsp90-S25 is essential for Atg1/Ulk1 activity

We next examined the impact of Hsp90 phosphorylation toward binding and kinase activity of Atg1/Ulk1. Using a proximity ligation assay (PLA), we observed the interaction of hHsp90α-FLAG and its S39 phosphomutants with Ulk1 in HEK293 cells (Figures 4A and S4A). As expected, WT-hHsp90α-FLAG was predominantly located in the cytoplasm, with faint staining observed in the nucleus. Importantly, neither the localization pattern of total hHsp90α-FLAG nor Ulk:hHsp90α-FLAG complexes were affected by the S39A or S39E mutation (Figures 4A and S4A). We next transiently expressed and immunoprecipitated hHsp90α-FLAG and the S39A and S39E mutants from HEK293 cells. Co-immunoprecipitation of Ulk1 was examined by immunoblotting, and our data showed a strong association between the non-phosphomutant hHsp90α-S39A compared with the WT hHsp90α and phosphomimetic S39E with Ulk1 (Figure 4B). This binding pattern was consistent when Ulk1-myc was co-expressed in mammalian cells (Figure S4B). Similar data were also obtained with yeast Atg1 (Figure 4C). We also showed this effect by briefly (20 min) treating the cells with rapamycin, thereby activating Ulk1 (Figure 4C). These data suggest that phosphomutants are able to mimic the non-phospho and the phospho form of hHsp90α. Previous works have shown that Atg1 autophosphorylation is coupled to its kinase activity.[51,52] We showed that while Atg1 is bound tightly to the non-phospho-mutant yHsp90-S25A-His_6, it does not have any kinase activity, as evidenced by its lack of autophosphorylation signal (Atg1 total phosphoserine and phosphothreonine status) (Figure 4C). Conversely, we did not observe binding of Atg1 to the phosphomimetic yHsp90-S25E-His_6, yet it had a very strong phosphoserine and phosphothreonine signal, indicating its kinase hyperactivity (Figure 4C). Furthermore, upon Atg1 activation by rapamycin treatment, it dissociated from WT yHsp90 and showed an increase in autophosphorylation (Figure 4C).

To gain a mechanistic understanding of the impact of Hsp90 toward Atg1/Ulk1 kinase activity, we conducted limited proteolysis-coupled mass spectrometry (LiP-MS) with recombinant hHsp90α and Ulk1 in the presence or absence of ATP. LiP-MS is a powerful approach by which altered proteolytic cleavage can be used to determine structural changes in a protein of interest induced by association with other proteins. Peptides with altered cleavage patterns under different conditions are termed “conformotypic peptides” and indicate a conformational change of the protein in this region[53] (Table S2). We have previously shown that regions of Hsp90 client proteins predicted to undergo local unfolding are also key regions for client protein interaction with Hsp90 and the chaperone machinery.[54] When comparing trypsin-digested Ulk1 protein in the presence or absence of hHsp90α, we identified peptides that structurally align with regions of local unfolding in other kinase clients that we have reported previously (Figures S5A–S5C).[54] Furthermore, when assessing the impact of ATP on the Ulk1:Hsp90 complex, we identified a single conformotypic Ulk1 peptide corresponding to residues 118-FLQQIAGAMRLL-129 (Figure 4D). Notably, the proteolytic sensitivity of this peptide was unchanged when comparing Ulk1 alone with Ulk1+ATP in the absence of Hsp90, confirming that the change is not

due solely to ATP binding to Ulk1 (Table S2). This conformotypic peptide is adjacent to the activation and catalytic loop of Atg1/Ulk1 (Figure 4D) and can potentially impact the kinase activity as a result of binding and phosphorylation of Hsp90 (Figure 4D). To test whether the identified conformotypic peptide is essential for Ulk1/Atg1 activation, we introduced mutations within the conformotypic peptide region of Atg1. First, we mutated the two conserved Ala residues (A157, A159) to Phe (M1). Additionally, we mutated the two conserved Gln residues (Q154, Q155) to Ala (M2). To test whether mutation of the conformotypic peptide had an impact on Atg1 activation, we immunoprecipitated (IP) Atg1-FLAG-WT and mutants from yeast cells that were treated with rapamycin or left untreated (Figure 4E). Consistent with our previous data, Atg1-WT had basal phosphorylation of Ser and Thr. Treatment with rapamycin increased p-Ser and p-Thr Atg1, which was coupled to dissociation from yHsp90. Notably, neither Atg1-M1 or -M2 showed an increase in phosphorylation following rapamycin treatment, suggesting that the conformotypic peptide is essential for the activity of Atg1.

Atg1/Ulk1-mediated phosphorylation of Hsp90 is essential for autophagy induction

To examine the impact of Atg1/Ulk1-mediated phosphorylation of Hsp90 on macroautophagy (referred to as autophagy), we measured the processing of a GFP-Atg8 fusion protein.[55] Atg8 is usually delivered into the lumen of vacuole[56–58] and degraded by vacuolar hydrolases. This leads to release of more stable GFP protein.[30,59] The level of free GFP is used as a measure of the autophagy activity present.[59] No processing of the GFP-Atg8 fusion was detectable in non-p-S25A cells (Figure 5A). In contrast, GFP-Atg8 processing was detectable in the phosphomimetic S25E mutant even in the absence of rapamycin treatment (Figure 5A). Deregulation of autophagy in these S25 phosphomutants was further corroborated by examination of the subcellular localization of the GFP fluorescence in these cells. In WT cells, the GFP-Atg8 is delivered to the vacuole, and the free GFP accumulates within the lumen of vacuole (Figure 5B). In contrast, no GFP fluorescence is detected in the vacuoles of the non-p-S25A mutant (Figure 5B). Conversely, in the phosphomimetic S25E mutant, Atg8 is incorporated into the autophagosome and transported to the vacuolar compartment even in the absence of rapamycin. This resulted in the presence of GFP fluorescence in the vacuoles of these cells (Figure 5B). We next asked whether the deregulation of autophagy in S25 phosphomutants is dependent or independent of the Atg1 kinase. Deletion of *ATG1* in the PP30 strain expressing either WT yHsp90 or its phosphomutant S25A or S25E completely impaired the autophagy activity as assessed by GFP-Atg8 immunoblotting and its accumulation to the vacuole (Figures 5C and 5D). In order to investigate the formation of pre-autophagosomal structures (PASs) in yeast, we introduced GFP-Atg17 to our yeast strains expressing yHsp90-WT, S25A, or S25E. We used the *ΔAtg1* strain expressing yHsp90-WT as a control. Localization of GFP-Atg17 to the vacuole (marked by FM4–64) indicates formation of a PAS complex.[60,61] We observed GFP-Atg17 puncta within the vacuole of yeast expressing yHsp90-WT only upon treatment with rapamycin, confirming the presence of PASs upon induction of autophagy. Consistent with our previous findings, GFP-Atg17 localization to the vacuole was not seen in yeast expressing yHsp90-S25A under any conditions, whereas yeast expressing yHsp90-S25E showed the formation of PAS even without rapamycin (Figure 5E). We next used the Pho8Δ60 assay to measure autophagic flux in yeast expressing the phosphomutants.

Deletion of the first 60 amino acids of Pho8 (Pho8Δ60) prevents its translocation into the endoplasmic reticulum; therefore, inactive Pho8Δ60 remains in the cytosol. Upon induction of autophagy, Pho8Δ60 is transported and activated in the vacuole as a part of autophagosomes. Therefore, Pho8Δ60 alkaline phosphatase (ALP) activity can be used as a readout for autophagy function.[62] Our data showed an increase in Pho8Δ60-derived ALP activity in WT yeast cells after autophagy was induced by 200 ng/mL rapamycin treatment for 4 h (Figure 5F). In contrast, the non-p-S25A mutant did not show an increase in ALP activity, whereas the phosphomimetic S25E had high ALP activity in the absence of rapamycin treatment (Figure 5F). To determine whether this phenomenon also occurs in mammalian cells, we examined LC3B conversion in HEK293 cells expressing hHsp90α-WT, S39A, or S39E. During autophagy, LC3B-I is converted into the lower-molecular-weight LC3B-II, which is correlated with the number of autophagosomes.[63,64] Consistent with our data from yeast, overexpression of hHsp90α-S39E, but not WT or S39A, resulted in increased conversion of LC3B-I to LC3B-II, indicating induction of autophagy (Figure 5G). In line with these findings, treatment with the lysosomal inhibitor Bafilomycin A (Baf A) led to increased LC3B conversion in cells expressing the control plasmid (empty vector [EV]), hHsp90α-WT, or S39A, whereas cells expressing hHsp90α-S39E had increased LC3B conversion even in the absence of Baf A (Figure 5H). Collectively, our results suggest the integral role of Atg1/Ulk1-mediated phosphorylation of Hsp90 in the autophagic pathway.

DISCUSSION

The molecular chaperone Hsp90 is subject to an array of PTMs, mostly by its client proteins, that regulate its chaperone function. This phenomenon is referred to as the chaperone code.[3] Here, we have shown that the autophagy-activating kinase Atg1/Ulk phosphorylates a conserved serine site (yHsp90-S25/hHsp90α-S39) within the amino domain of Hsp90. Data from our orthogonal approaches have revealed the significance of this phosphorylation in regulation of Hsp90 function and chaperoning of its clients, including Atg1/Ulk1.

Atg1/Ulk1 is an Hsp90 client, and inhibition of Hsp90 causes degradation of Atg1/Ulk1.[36] Our findings here suggest that this is due to Hsp90 binding to and insulation of Atg1/Ulk1 at steady state (Figure 6). Further, our data suggest that upon activation by environmental cues, Atg1/Ulk phosphorylates Hsp90 and inhibits its ATPase activity, which leads to dissociation of the Atg1/Ulk1:Hsp90 complex. Using standardized methods as recommended by the autophagy scientific community,[31] we evaluated the ability of Hsp90 phosphomutants to promote the initiation of autophagy. Our results indicated that Atg1/Ulk1 phosphorylation of Hsp90 triggers the release and autophosphorylation of Atg1/Ulk1 and the subsequent activation of autophagy (Figure 6). To gain insight into this process at the structural level, we assessed the impact of ATP on the Ulk1:Hsp90 complex by LiP-MS and identified a conformotypic peptide that is adjacent to the activation and catalytic loops of Atg1/Ulk1 (Figure 4). This finding supports our model, as this conformational change likely impacts the kinase activity as a result of phosphorylation of and dissociation from Hsp90.

Previous work has reported the mutation of S25 to proline had little effect on Hsp90 ATPase activity, and it could not be stimu lated by the co-chaperone Aha1.[44] Although this mutant

had an elevated heat shock response, it had a slight negative impact on activity of the kinase client v-Src. Our findings here have shown that mutation of S25 to non-phosphorylatable S25A or phosphomimetic S25E also has an opposite effect on the activity of kinase versus non-kinase clients. While non-phospho-mutant S25A led to hyperactivity of typical kinase clients (v-Src, Slt2, and Ste11), non-kinase client activity (Hsf1, GR, ERα, AR) was negatively impacted. Conversely, non-kinase clients had significantly higher activity in the presence of phosphomimetic yHsp90-S25E, whereas kinase clients were inhibited, potentially due to a slow chaperone cycle of this mutant, as different ATP hydrolysis rates may favor certain classes of clients.[65–68]

Although it is tempting to use global analysis to identify phosphorylation sites on proteins of interest, this does not appear to be an efficient strategy for understanding Hsp90 functional regulation. Our study highlights the complexity of Hsp90 PTMs and the importance of detailed investigation of each PTM and its consequences toward Hsp90 chaperone function and regulation of different cellular processes. Here, we have shown how phosphorylation of a single residue on Hsp90 controls a cellular process. As Hsp90 functions in many cellular processes, namely signaling pathways, our work emphasizes the importance of detailed studies of PTMs to dissect their physiological impact at the cellular level individually.

Hsp90 is subject to additional regulatory mechanisms by co-chaperones, many of which are themselves regulated by PTM,[7] which poses an additional challenge toward understanding the impact of PTMs on regulating the global chaperone function. Further exploration of post-translational regulation of Hsp90 and its co-chaperones may unravel additional cellular processes that depend on Hsp90. Many of the well-known Hsp90-dependent pathways are those that are dysregulated in cancer, and as such, Hsp90 inhibitors have gone through extensive testing and development in both the pre-clinical and clinical settings.[14,69,70] Additionally, pimitespib (Jeselhy, TAS-116), an Hsp90 inhibitor, has recently been shown to meet its primary endpoint in a randomized phase III clinical trial, and it has been approved for treatment of advanced gastrointestinal stromal tumor (GIST) in Japan.[71] This is an important milestone in the development of Hsp90 inhibitors. Therefore, a complete understanding of the direct role of Hsp90 in various cellular processes and how Hsp90 function in these pathways is regulated may provide clues as to how and when Hsp90 inhibitors will be most successful for treatment of diseases, such as human cancer.

Limitations of the study

Our data in yeast expressing phosphomutant-Hsp90-S25A or-S25E show a broad impact on kinase and non-kinase clients stability and/or activity, indicating how this point mutation impacts Hsp90 chaperone function. Based on the data presented here that Ulk1 specifically phosphorylates this residue of Hsp90, we speculate that in a cellular context with mixed populations of Hsp90, only Ulk1 activity would be impacted by this phosphorylation. We suspect that Ulk1-mediated phosphorylation of Hsp90 is part of a regulatory feedback loop in which Hsp90 chaperones Ulk1, and Ulk1 in turn phosphorylates Hsp90, triggering release of the active kinase and resetting the chaperone cycle without impacting other Hsp90 clients. However, there are technical considerations that can require further validation of the results in mammalian cells. Principally, HEK293 cells used in this study express endogenous

Hsp90α, which has activity that would contribute to the results related to the induction of autophagy.

STAR★METHODS

RESOURCE AVAILABILITY

Lead contact—Further information and requests for resources and reagents should be directed to and will be fulfilled by the lead contact, Mehdi Mollapour (mollapom@upstate.edu).

Materials availability—Plasmids generated in this study will be made available on request, but we may require a payment and/or a completed materials transfer agreement if there is potential for commercial application.

Data and code availability—The mass spectrometry proteomics data have been deposited to the ProteomeXchange Consortium via the PRIDE[84] partner repository and are publicly available as of the date of publication. Accession numbers are listed in the key resources table. This paper does not report original code. Any additional information required to reanalyze the data reported in this paper is available from the lead contact upon request.

EXPERIMENTAL MODEL AND STUDY PARTICIPANT DETAILS

Cell lines—Cultured human embryonic kidney (HEK293) cells were grown in Dulbecco's Modified Eagle Medium (DMEM, Sigma-Aldrich), parental (WT) and Ulk1 KO HAP1 cells were cultured in Isocove's Modified Dulbecco's Medium (IMDM; Gibco) and DLD-1 cells were grown in RPMI 1640 (Sigma-Aldrich). All growth media was supplemented with 10% fetal bovine serum (FBS, Sigma-Aldrich). HEK293 cells were acquired from (American Type Culture Collection, ATCC), HAP1 and DLD-1 cells were purchased from Horizon Discovery. Cells were maintained in a CellQ incubator (Panasonic Healthcare) at 37°C in an atmosphere containing 5% CO_2.

Plasmids—Atg1-FLAG was constructed by PCR from pRS406-Atg1 (Addgene # 166846) by amplifying *ATG1* and the flanking region (−974bp to +460bp) using the primers ATG1-NOT1-F and ATG1-NOT1-R (Table S3). The PCR product was inserted into the pRS416 vector using restriction digest with NotI. DYKDDDDK (FLAG) was inserted at the 3′ end by mutagenesis using the primers ATG1-FLAG-F and ATG1-FLAG-R (Table S3). Hsp82-His_6 with a PreScission protease cleavage site introduced between the amino-domain and charged linker region was cloned previously.[37,38] pRK5-Ulk1-myc (#31961), GFP-Atg8 (#49425), pJK59-GFP-Atg17 (#44175) and ptfLC3 (#21074) were purchased from Addgene.

pHCA/rGR,[75] constitutively expressing glucocoticoid receptor (GR) under control of the Alcohol dehydrogenase promoter (*ADH1*), the GRE reporter vector pΔS26X, a *URA3* vector which expresses β-galactosidase (encoded by *lacz*) as a reporter gene under control of a promoter bearing 3×GR response elements[76] was reported previously.[80] V5-ERα and V5-AR constitutively expressing estrogen receptor-alpha (ERα) and androgen receptor (AR),

respectively, under control of the Glycerol-3-Phosphate Dehydrogenase (*GPD1*) promoter were previously described.[77] pUCdeltaSS-ERE,[78] 2x*RLM1-LacZ* reporter plasmid,[47] 4XHSE-*LacZ*-pUp41a,[47] YpRS426-*GAL1-v-Src* plasmid,[79] STE11ΔN-myc-pYES2,[80] and pcDNA3-Cdc37-FLAG WT[81] were all reported previously. Point mutations were made using site-directed mutagenesis (see Table S3) and confirmed by DNA sequencing.

Yeast strains—The yeast strain pp30 (*MAT*a, *trp1–289, leu2–3,112, his3–200, ura3–52, ade2–101, lys2–801, hsc82KANMX4, hsp82KANMX4*) expressing *HSP82-His$_6$ (yHSP90)*-Ycplac111 as the sole Hsp90 was used in this study. These yeast strains were reported previously.[4] *ATG1* was deleted in these strains by using ATFDEL and ATRDEL primers and pAG25 (selection marker nourseothricin resistance gene clonNAT) to PCR 50bp upstream and downstream of *ATG1* gene. The PCR product was then used to transform PP30 stains expressing Hsp82-His$_6$ or the phosphomutants Hsp82-His$_6$-S25A or Hsp82-His$_6$-S25E. Colonies resistant to 200μg/ml nourseothricin were selected and used to confirm *ATG1* deletion by PCR reacting using ATFOR and ATREV primers.[85] Wild type *ATG1* gene yielded a product of 3188bp where as the Δ*atg1* 1883bp. The 5′ and 3′ junction were also checked by PCR using primers 5’ = NATF3 and ATREV; 3’ = NATR and ATFOR.

METHOD DETAILS

Yeast growth media—Yeast cells were grown on YPDA (2% (w/v) Bacto peptone, 1% yeast extract, 2% glucose, 20 mg/L adenine), YPGal (2% (w/v) Bacto peptone, 1% yeast extract, 2% galactose, 20 mg/L adenine) and YPRaf (2% (w/v) Bacto peptone, 1% yeast extract, 2% raffinose, 20 mg/L adenine). Selective growth was on dropout 2% glucose (DO) medium with appropriate amino acids.[86] Medium pH was adjusted to 6.8 with NaOH before autoclaving.

Protein purification—Wild type and mutant forms of Hsp90 and co-chaperones of Hsp90 were expressed as previously described with His$_6$-tags.[87,88] Briefly, we used Talon affinity chromatography Superdex 75 or 200 PG, as appropriate, for gel filtration chromatography and finally Q-sepharose ion-exchange chromatography.

***In vitro* kinase assay—**Bacterially expressed and purified hHsp90α-His$_6$ and the non-phosphomutant S39A were bound to Ni-NTA agarose and then resuspended in 40μL protein kinase buffer (PK buffer) consists of 50mM Tris HCl pH7.5, 10mM MgCl2, 0.1mM EDTA, 2mM DTT. Each reaction also contained 20–30ng of recombinant Ulk1 (0.5 μg/μL; ab95322, Abcam) followed by adding 0.2 mM ATP final concentration and incubation at 30°C for 10 min. The reaction was quenched by addition of 40μL of protein loading buffer, boiling of samples for 3 min, followed by immunoblotting.[5]

Protein extraction from yeast—Yeast cells were collected from liquid culture by centrifugation and resuspended in 500μL of protein extraction buffer (20mM Tris-HCl (pH 7.4), 500 mM NaCl, 1 mM $MgCl_2$, protease inhibitor cocktail (Roche), and PhosSTOP (Roche)) and two pellet volumes of acid washed glass beads as previously described.[4] To lyse the cells, tubes were agitated using a bead beater (mini-Beadbeater 8, Bio-spec Products, USA) for 30 s at maximum speed and then 30 s on ice. This procedure was

repeated 6X followed by (10,000Xg; 5 s) to pellet the beads and unbroken cells. The supernatant was transferred to a new microfuge tube and centrifuged (10,000Xg; 10 min) to pellet insoluble aggregates. Supernatant was then transferred to a fresh microfuge.

Protein extraction from mammalian cells—Protein extraction from mammalian cells was carried out using methods previously described.[4] Adherent cells were washed with ice-cold PBS and lysed with 200μL lysis buffer (20mM Tris-HCl (pH 7.4), 100 mM NaCl, 1 mM $MgCl_2$, 0.1% NP40, protease inhibitor cocktail (Roche), and PhosSTOP (Roche)). Cells were briefly sonicated and centrifuged at 4°C, 10,000Xg for 8 min to pellet cell debris. The supernatant (cell lysate) was transferred to a fresh tube and stored at −80°C or used in downstream assays.

Pulldown, immunoprecipitation (IP) and immunoblotting—For pulldown, yeast cell lysates were incubated with Ni-NTA agarose (Qiagen) for 2 h 4°C or anti-FLAG antibody conjugated agarose beads (Sigma) for 2 h at 4°C. Protein bound to beads was washed with fresh extraction buffer 4 times and eluted in 5x Laemmli buffer. Precipitated proteins were separated by SDS-PAGE and transferred to nitrocellulose membranes. IP of protein from mammalian cells was performed as above with anti-FLAG conjugated agarose beads.

Co-precipitated proteins and inputs were detected by immunoblotting with antibodies recognizing FLAG, 6x-His (ThermoFisher Scientific), phos-(Ser/Thr)-Phe, GAPDH, HOP, hCdc37, Ulk1, myc-tag, LC3B (Cell Signaling), phosphoserine, phospho-threonine, FLAG (Sigma-Aldrich), GFP (BioLegend) tubulin (Abcam) phosphotyrosine, v-Src (Millipore), p23 (ENZO Life Sciences), hAha1 (StressMarq Biosciences), $Sti1^{Hop}$ (a kind gift from Dr. Daniel C. Masison, NCI, USA), $Cdc37^{p50}$ and yAha1 (a kind gift from Dr Len Neckers, NCI, USA), Sba1 (Institute of Cancer Research, UK). Secondary antibodies raised against mouse, rabbit, and rat (Cell Signaling) and anti-mouse Alexa Fluor 488 (ThermoFisher were also used (See Key Re-sources Table).

PreScission protease cleavage and immunoblotting—PreScission Protease cleavage was achieved by incubating $yHsp90His_6$ bound to Ni-NTA agarose with 10 units of PreScission Protease in 50mM Tris-HCl, 150mM NaCl, 1 M EDTA, 1mM DTT (pH 7.0) at 5°C for 2hr.

Non-essential yeast kinase delete screen—EUROSCARF collection of haploid non-essential kinase deletes in BY4741 (*MAT* a; Δ*his3*-Δ*1; leu2*-Δ*0; met15*-Δ*0; ura3*-Δ*0*) background (www.uni-frankfurt.de/fb15/mikro/euroscarf/) was used to screen for S25 phosphorylation (Table S1). These stains were transformed with $yHsp90His_6$-Ycplac111. The wild type BY4741 was also transformed with the same construct as well as the S25A mutant. These mutants were grown in liquid DO media with appropriate amino acids in 96-well plate. Cells were centrifuged at 4000 RPM for 5min and then washed with ice-cold TBS. Pellet were then resuspended in 50μL of protein loading buffer (10% SDS, 500Mm DTT, 50% Glycerol, 500mM Tris-HCL and 0.05% bromophenol blue dye) and then boiled for 5min followed by centrifugation at 4000 RPM for 5min. The lysate was spotted on

nitrocellulose membrane 10 times and then probed with either anti-6x-His (ThermoFisher Scientific) or anti-phospho-(Ser/Thr) Phe (Cell Signaling) antibodies.

ATPase activity measurements—ATPase assays were conducted using the pyruvate kinase-lactate dehydrogenase assay as previously described (Panaretou et al., 1998).

Isothermal titration calorimetry and K_d measurements—Heat of interaction was measured on an ITC200 microcalorimeter (Microcal) under the buffer conditions 20mM Tris, pH 7.5, containing 5mM NaCl and 6mM $MgCl_2$ for AMPPNP binding experiments. For AMPPNP interactions, 20 aliquots of 14.8μL of 1mM AMPPNP were injected into 50μM wild type yHsp90 or mutant S25A or S25E. In contrast, for Aha1 experiments we injected 10 aliquots of 400μM Aha1 into 30μM Hsp90. Heat of dilution was determined in a separate experiment by diluting protein or ligand into buffer, and the corrected data fitted using a nonlinear least square curve-fitting algorithm (Microcal Origin) with three floating variables: stoichiometry, binding constant and change in enthalpy of interaction. Heat of interaction was measured on an MSC system (Microcal), with a cell volume of 1.458mL, under the buffer conditions 20mM Tris pH 8.0 containing 1mM EDTA, 5mM NaCl and 7mM $MgCl_2$ at 30°C.

Yeast Hsp90 client activity assays—Expressed *STE11*Δ*N*-cMYC[80] and v-Src proteins were detected with Myc mouse antibody (Cell signaling Technology) and EC10 mouse antibody (Millipore) respectively. v-Src activity with 4G10 mouse anti-phosphotyrosine (Millipore). β-galactosidase assay for measuring GRE-*LacZ* expression,[75] ERE-*LacZ*,[78] HSE-*LacZ* expression,[89] and RLM1-*LacZ*[47,77]. Note that GRE-*LacZ* reporter was also used to measure AR activity.[78]

β-Galactosidase assay—Yeast cells expressing the appropriate steroid hormone receptors; *GR, AR, ER* and their element-*Lac*-Z reporter were grown overnight to exponential phase with a cell density of $2–3\times10^6$ cells/mL in 50mL of the same medium at 30°C. Then, 30μM dexamethasone (DEX), 20nM Dihydrotestosterone (DHT), or 200nM β-Estradiol was added to a final concentration followed by incubation at 30°C for 2.5 h before measurement of Steroid Hormone Receptor-*LacZ* activity. Heat shock element (HSE)-*LacZ* expressing yeast cells were heat shocked at 39°C for 40 min. RLM1-*LacZ* expressing cells were stressed with 8mM caffeine for 4 h. Cells were collected by centrifugation (2000×g; 5 min), washed once with dH_2O, and frozen at −80°C. β-Galactosidase activity was measured as previously described.[5,77] Cell lysate (10μL) was mixed with equal volume of 2XZ-buffer (60mM Na_2HPO_4, 60mM NaH_2PO_4, 5mM KCl, 0.5mM $MgSO_4$, pH adjusted to 7.0). The mixture was added to 700μL of 2 mg/mL ONPG solution (O-Nitrophenyl-β-D-galactopyranoside dissolved in 1X Z buffer) prewarmed at 30°C. The reaction was stopped by adding 500μL of 1M Na_2CO_3. The optical density at 420nm (OD_{420}) of each reaction mixture was determined. The protein concentration of the lysate was determined by the BioRad Bradford assay. The β-Galactosidase activity was calculated using the following formula: Enzyme activity = $1000\times OD_{420}$/minute/[10μL3protein concentration(μg/μL)].

Proximity ligation assay (PLA)—PLA was performed using manufacturers protocol (Sigma-Aldrich) as previously described.[90] HEK293 cells were plated overnight on glass

coverslips and then transiently transfected with pcDNA3-EV, pcDNA3-hHsp90α-FLAG-WT, S39A or S39E overnight. Cells were fixed in 4% paraformaldehyde for 20 min at room temperature, washed 3x with fresh PBS+ (1X PBS, 1mM MgCl2, 1mM $CaCl_2$, pH 7.4), and then permeabilized with 0.2% Triton X-100 at room temperature for 4 min followed 3 washes with fresh PBS+. Samples were incubated with Duolink Blocking Solution in a humidity chamber for 1 h at 37°C (Sigma-Aldrich). Rabbit anti-Ulk1 (Cell Signaling Technology) and mouse anti-FLAG (Sigma-Aldrich) were diluted 1:100 in Duolink Antibody Diluent (DUO82008; Sigma-Aldrich) and applied to coverslips. Coverslips were incubated in a humidity chamber 1 h at 37°C. Coverslips were washed 2X with Duolink Wash Buffer A (Sigma-Aldrich). Duolink anti-mouse (MINUS) (Sigma-Aldrich) and anti-rabbit (PLUS) (Sigma-Aldrich) probes were diluted in Duolink antibody diluent according to manufacturer's instructions and in incubated in a humidity chamber 1 h at 37°C. Coverslips were washed 2X with Duolink Wash Buffer A. Coverslips were incubated with Duolink ligase enzyme according to manufacturer's instructions then washed 2X with Duolink Wash Buffer A. Samples were incubated with anti-mouse Alexa Fluor 488 (ThermoFisher) secondary antibody at 1:900 dilution for 45 min followed by two washes in Wash Buffer A. Duolink In Situ Detection Reagents Red (Sigma-Aldrich) were used for signal amplification and detection according to manufacturer's instruction. Coverslips were washed twice with 1X Wash Buffer B followed by one wash with 0.01X Wash Buffer B. Coverslips were mounted onto slides using Duolink In Situ Mounting Medium with DAPI (Sigma-Aldrich). Images were obtained using a Leica TCS SP8 confocal microscope. Image analysis was done with the ImageJ V2.1.0/1.53c program.

Limited proteolysis coupled mass spectrometry analysis—Limited proteolysis of Ulk1 was achieved by exposing 10μg recombinant Ulk1 (0.5 μg/μL; ab95322, Abcam) with 1.0 μg recombinant Hsp90α and 200μM of ATP (preincubated on ice) to 2.0 μg/mL TPCK-treated trypsin (Sigma) for 6 min on ice, as previously described.[91] Digest was loaded onto an SDS-PAGE gel and following Coomassie staining visible bands were manually cut into small pieces approximately 1 mm × 1 mm. The selected protein gel bands were in-gel digested with chymotrypsin and the tryptic peptides were desalted and subjected to LC-MS/MS. The mass spec data was processed by MaxQuant and proteins were identified by database searching with Uniprot human database. Data are presented in (Table S2).

Pho8Δ60 assay (ALP assay)—The Pho8Δ60 assay is a quantitative enzymatic assay to monitor bulk autophagy. Phos8S1 and Pho8S4 primers and clonNAT (pYM-N15; nourseothricin resistance) from EUROSCARF (http://web.uni-frankfurt.de/fb15/mikro/euroscarf/data/Knop.html) were used to PCR amplify a product containing the constitutive GPD1 promoter and selection marker clonNAT flanked by 40 nucleotides just upstream of the initiation codon of the PHO8 gene and 40 nucleotides downstream of amino acid 60. The PCR product was then used to transform PP30 stain expressing Hsp82-His_6 or the phosphomutants Hsp82-His_6-S25A or Hsp82-His_6-S25E and also containing the wild type *PHO8* gene. Colonies resistant to 200μg/mL nourseothricin were selected and used to confirm if the PHO8 gene was correctly replaced with nourseothricin marker, GPD1 promoter and pho8Δ60, which lacks first 60 amino acid of PHO8 by PCR using Pho8S2 and Pho8S3 primers. Yeast strains harboring Pho8Δ60 gene were grown on liquid YPD to mid-

log phase (O.D.600 = 0.5 to 1) for at least over 3 doubling time. For induction of autophagy, rapamycin (200 ng/mL final concentration) was added to the culture media and incubated for 4 h. Cells were centrifuged at 1500 g for 3 min and washed with ice-cold water. Yeast cells pellets were suspended in 0.2 mL of ice-cold assay buffer (100 mM of Tris-HCl, pH 9.0; 10 μM of $MgSO_4$, and 10 mM of $ZnSO_4$) and the suspension was transferred to a 1.5-mL microcentrifuge tube. Acid-washed glass beads (425–600 μm) were added to the level of the interface. Tubes were placed on ice for at least 5 min, then vigorously mixed by the beads-beater (6 × 30 s), placing for at least 30 s intervals on ice in between the mixing. Additional 0.2 mL of assay buffer was added, mixed, and centrifuged at 14,000 g for 1 min 0.3 mL of the supernatant fraction were transferred to a new 1.5-mL microcentrifuge tube. 0.05 mL of the cell lysate solution was added to a 0.45 mL with assay buffer in new tube and then prewarmed into a 30°C water bath for at least 1 min. Assy was initiated by addition of 0.05 mL of 55 mM α-naphthyl phosphate disodium salt dissolved in assay buffer, mixed well, and incubated at 30°C for 20 min. Reaction was stopped by addition of 0.5 mL of stop buffer (2 M glycine-NaOH (pH 11.0)). Fluorescence was measured at wavelength of 345 nm for excitation and 472 nm for emission. Protein concentration of the cell lysate was also determined using Bradford assay. ALP activity is presented as emission per the amount of protein in the reaction (mg) and the reaction time (min).

Vacuole staining and fluorescence microscopy—PP30 stains expressing yHsp90-His_6-WT or the phosphomutants Hsp82-His_6-S25A or Hsp82-His_6-S25E as well as GFP-Atg8 or GFP-Atg17 grown to mid-log on YPDA and then treated either with or without rapamycin (200 ng/mL final concentration) for 2 h followed by vascular staining with 8mM FM4–64 (Invitrogen) at 30°C for 30 min. Live cells were washed with YPDA and then immediately visualized using a Revolve R4 Microscopy System (Discover Echo Inc.) with GFP and red filters. Images were captured using ECHO imaging software (Discover Echo Inc.).

QUANTIFICATION AND STATISTICAL ANALYSIS

Densitometry was performed using ImageStudioLite v5.2.5 to quantify immunoblot band signal intensity. All statistics were performed using GraphPad Prism version 9.2.0 for macOS (GraphPad Software, La Jolla, California, USA, www.graphpad.com). Statistical significance was ascertained between individual samples using a Student's t-test or Tukey's multiple comparisons test where indicated. Significance was denoted as asterisks in each figure: *$p < 0.05$; **$p < 0.01$; ***$p < 0.001$; ****$p < 0.0001$. Error bars represent the standard deviation (S.D.) for three independent experiments.

PREPARATION OF FIGURES Some Figure panels were prepared using BioRender software (https://biorender.com/).

Supplementary Material

Refer to Web version on PubMed Central for supplementary material.

ACKNOWLEDGMENTS

We are grateful to Dr. Daniel J Klionsky (University of Michigan) for their constructive comments. This work was supported by the National Institute of General Medical Sciences of the National Institutes of Health under award number R35GM139584 (M.M.). The content is solely the responsibility of the authors and does not necessarily represent the official views of the National Institutes of Health. This work was also supported with funds from the SUNY Upstate Medical University and Upstate Foundation. Figure 6 was created with BioRender.com.

REFERENCES

1. Schopf FH, Biebl MM, and Buchner J. (2017). The HSP90 chaperone machinery. Nat. Rev. Mol. Cell Biol. 18, 345–360. 10.1038/nrm.2017.20. [PubMed: 28429788]
2. Taipale M, Krykbaeva I, Koeva M, Kayatekin C, Westover KD, Karras GI, and Lindquist S. (2012). Quantitative analysis of HSP90-client interactions reveals principles of substrate recognition. Cell 150, 987–1001. 10.1016/j.cell.2012.06.047. [PubMed: 22939624]
3. Backe SJ, Sager RA, Woodford MR, Makedon AM, and Mollapour M. (2020). Post-translational modifications of Hsp90 and translating the chaperone code. J. Biol. Chem. 295, 11099–11117. 10.1074/jbc.REV120.011833. [PubMed: 32527727]
4. Mollapour M, Tsutsumi S, Donnelly AC, Beebe K, Tokita MJ, Lee MJ, Lee S, Morra G, Bourboulia D, Scroggins BT, et al. (2010). Swe1Wee1-dependent tyrosine phosphorylation of Hsp90 regulates distinct facets of chaperone function. Mol. Cell. 37, 333–343, S1097–2765(10)00030–4 [pii]. 10.1016/j.molcel.2010.01.005. [PubMed: 20159553]
5. Woodford MR, Truman AW, Dunn DM, Jensen SM, Cotran R, Bullard R, Abouelleil M, Beebe K, Wolfgeher D, Wierzbicki S, et al. (2016). Mps1 Mediated Phosphorylation of Hsp90 Confers Renal Cell Carcinoma Sensitivity and Selectivity to Hsp90 Inhibitors. Cell Rep. 14, 872–884. 10.1016/j.celrep.2015.12.084. [PubMed: 26804907]
6. Solier S, Kohn KW, Scroggins B, Xu W, Trepel J, Neckers L, and Pommier Y. (2012). Feature Article: Heat shock protein 90alpha (HSP90alpha), a substrate and chaperone of DNA-PK necessary for the apoptotic response. Proc. Natl. Acad. Sci. USA 109, 12866–12872, 1203617109 [pii]. 10.1073/pnas.1203617109. [PubMed: 22753480]
7. Backe SJ, Woodford MR, Ahanin E, Sager RA, Bourboulia D, and Mollapour M. (2023). Impact of Co-chaperones and Posttranslational Modifications Toward Hsp90 Drug Sensitivity. Subcell. Biochem. 101, 319–350. 10.1007/978-3-031-14740-1_11. [PubMed: 36520312]
8. Biebl MM, and Buchner J. (2019). Structure, Function, and Regulation of the Hsp90 Machinery. Cold Spring Harbor Perspect. Biol. 11, a034017. 10.1101/cshperspect.a034017.
9. Dean ME, and Johnson JL (2021). Human Hsp90 co-chaperones: perspectives on tissue-specific expression and identification of co-chaperones with similar in vivo functions. Cell Stress Chaperones 26, 3–13. 10.1007/s12192-020-01167-0. [PubMed: 33037995]
10. Ali MMU, Roe SM, Vaughan CK, Meyer P, Panaretou B, Piper PW, Prodromou C, and Pearl LH (2006). Crystal structure of an Hsp90-nucleotide-p23/Sba1 closed chaperone complex. Nature 440, 1013–1017, nature04716 [pii]. 10.1038/nature04716. [PubMed: 16625188]
11. Verba KA, Wang RYR, Arakawa A, Liu Y, Shirouzu M, Yokoyama S, and Agard DA (2016). Atomic structure of Hsp90-Cdc37-Cdk4 reveals that Hsp90 traps and stabilizes an unfolded kinase. Science 352, 1542–1547. 10.1126/science.aaf5023. [PubMed: 27339980]
12. Prodromou C, Roe SM, O'Brien R, Ladbury JE, Piper PW, and Pearl LH (1997). Identification and structural characterization of the ATP/ADP-binding site in the Hsp90 molecular chaperone. Cell 90, 65–75. S0092–8674(00)80314–1 [pii]. [PubMed: 9230303]
13. Prodromou C, Roe SM, Piper PW, and Pearl LH (1997). A molecular clamp in the crystal structure of the N-terminal domain of the yeast Hsp90 chaperone. Nat. Struct. Biol. 4, 477–482. [PubMed: 9187656]
14. Neckers L, and Workman P. (2012). Hsp90 molecular chaperone inhibitors: are we there yet? Clin. Cancer Res. 18, 64–76, 18/1/64 [pii]. 10.1158/1078-0432.CCR-11-1000. [PubMed: 22215907]
15. Schulte TW, Akinaga S, Soga S, Sullivan W, Stensgard B, Toft D, and Neckers LM (1998). Antibiotic radicicol binds to the N-terminal domain of Hsp90 and shares important biologic activities with geldanamycin. Cell Stress Chaperones 3, 100–108. [PubMed: 9672245]

16. Hainzl O, Lapina MC, Buchner J, and Richter K. (2009). The charged linker region is an important regulator of Hsp90 function. J. Biol. Chem. 284, 22559–22567, M109.031658 [pii]. 10.1074/jbc.M109.031658. [PubMed: 19553666]

17. Tsutsumi S, Mollapour M, Prodromou C, Lee CT, Panaretou B, Yoshida S, Mayer MP, and Neckers LM (2012). Charged linker sequence modulates eukaryotic heat shock protein 90 (Hsp90) chaperone activity. Proc. Natl. Acad. Sci. USA 109, 2937–2942, 09 [pii].. 10.1073/pnas.1114414109 [PubMed: 22315411]

18. Nemoto T, Matsusaka T, Ota M, Takagi T, Collinge DB, and Walther-Larsen H. (1996). Dimerization characteristics of the 94-kDa glucose-regulated protein. J. Biochem. 120, 249–256. [PubMed: 8889807]

19. Richter K, Muschler P, Hainzl O, and Buchner J. (2001). Coordinated ATP hydrolysis by the Hsp90 dimer. J. Biol. Chem. 276, 33689–33696. 10.1074/jbc.M103832200M103832200 [pii]. [PubMed: 11441008]

20. Prodromou C, and Pearl LH (2003). Structure and functional relationships of Hsp90. Curr. Cancer Drug Targets 3, 301–323. [PubMed: 14529383]

21. Wayne N, and Bolon DN (2007). Dimerization of Hsp90 is required for in vivo function. Design and analysis of monomers and dimers. J. Biol. Chem. 282, 35386–35395, M703844200 [pii]. 10.1074/jbc.M703844200. [PubMed: 17908693]

22. Young JC, Obermann WM, and Hartl FU (1998). Specific binding of tetratricopeptide repeat proteins to the C-terminal 12-kDa domain of hsp90. J. Biol. Chem. 273, 18007–18010. [PubMed: 9660753]

23. Carrello A, Ingley E, Minchin RF, Tsai S, and Ratajczak T. (1999). The common tetratricopeptide repeat acceptor site for steroid receptor-associated immunophilins and hop is located in the dimerization domain of Hsp90. J. Biol. Chem. 274, 2682–2689. [PubMed: 9915798]

24. Russell LC, Whitt SR, Chen MS, and Chinkers M. (1999). Identification of conserved residues required for the binding of a tetratricopeptide repeat domain to heat shock protein 90. J. Biol. Chem. 274, 20060–20063. [PubMed: 10400612]

25. Ramsey AJ, Russell LC, Whitt SR, and Chinkers M. (2000). Overlapping sites of tetratricopeptide repeat protein binding and chaperone activity in heat shock protein 90. J. Biol. Chem. 275, 17857–17862. 10.1074/jbc.M001625200M001625200 [pii]. [PubMed: 10751404]

26. Graf C, Stankiewicz M, Kramer G, and Mayer MP (2009). Spatially and kinetically resolved changes in the conformational dynamics of the Hsp90 chaperone machine. EMBO J. 28, 602–613, emboj2008306 [pii]. 10.1038/emboj.2008.306. [PubMed: 19165152]

27. Mickler M, Hessling M, Ratzke C, Buchner J, and Hugel T. (2009). The large conformational changes of Hsp90 are only weakly coupled to ATP hydrolysis. Nat. Struct. Mol. Biol. 16, 281–286, nsmb.1557 [pii]. 10.1038/nsmb.1557. [PubMed: 19234469]

28. Csermely P, Kajtár J, Hollósi M, Jalsovszky G, Holly S, Kahn CR, Gergely P Jr., Söti C, Mihály K, and Somogyi J. (1993). ATP induces a conformational change of the 90-kDa heat shock protein (hsp90). J. Biol. Chem. 268, 1901–1907. [PubMed: 8420964]

29. Hessling M, Richter K, and Buchner J. (2009). Dissection of the ATP-induced conformational cycle of the molecular chaperone Hsp90. Nat. Struct. Mol. Biol. 16, 287–293, nsmb.1565 [pii]. 10.1038/nsmb.1565. [PubMed: 19234467]

30. Torggler R, Papinski D, and Kraft C. (2017). Assays to Monitor Autophagy in Saccharomyces cerevisiae. Cells 6. 10.3390/cells6030023.

31. Klionsky DJ, Petroni G, Amaravadi RK, Baehrecke EH, Ballabio A, Boya P, Bravo-San Pedro JM, Cadwell K, Cecconi F, Choi AMK, et al. (2021). Autophagy in major human diseases. EMBO J. 40, e108863. 10.15252/embj.2021108863.

32. Rios J, Sequeida A, Albornoz A, and Budini M. (2020). Chaperone Mediated Autophagy Substrates and Components in Cancer. Front. Oncol. 10, 614677. 10.3389/fonc.2020.614677.

33. Delorme-Axford E, Guimaraes RS, Reggiori F, and Klionsky DJ (2015). The yeast Saccharomyces cerevisiae: an overview of methods to study autophagy progression. Methods 75, 3–12. 10.1016/j.ymeth.2014.12.008. [PubMed: 25526918]

34. Turco E, Fracchiolla D, and Martens S. (2020). Recruitment and Activation of the ULK1/Atg1 Kinase Complex in Selective Autophagy. J. Mol. Biol. 432, 123–134. 10.1016/j.jmb.2019.07.027. [PubMed: 31351898]
35. Soroka J, and Buchner J. (2012). Mechanistic aspects of the Hsp90 phosphoregulation. Cell Cycle 11, 1870–1871, 20418 [pii]. 10.4161/cc.20418. [PubMed: 22544316]
36. Joo JH, Dorsey FC, Joshi A, Hennessy-Walters KM, Rose KL, McCastlain K, Zhang J, Iyengar R, Jung CH, Suen DF, et al. (2011). Hsp90-Cdc37 chaperone complex regulates Ulk1- and Atg13-mediated mitophagy. Mol. Cell. 43, 572–585. 10.1016/j.molcel.2011.06.018. [PubMed: 21855797]
37. Mollapour M, Tsutsumi S, Truman AW, Xu W, Vaughan CK, Beebe K, Konstantinova A, Vourganti S, Panaretou B, Piper PW, et al. (2011). Threonine 22 phosphorylation attenuates hsp90 interaction with co-chaperones and affects its chaperone activity. Mol. Cell. 41, 672–681, S1097–2765(11)00094–3 [pii]. 10.1016/j.molcel.2011.02.011. [PubMed: 21419342]
38. Mollapour M, Tsutsumi S, Kim YS, Trepel J, and Neckers L. (2011). Casein kinase 2 phosphorylation of Hsp90 threonine 22 modulates chaperone function and drug sensitivity. Oncotarget 2, 407–417. [pii]. [PubMed: 21576760]
39. Li R, Yuan F, Fu W, Zhang L, Zhang N, Wang Y, Ma K, Li X, Wang L, Zhu WG, and Zhao Y. (2017). Serine/Threonine Kinase Unc-51-like Kinase-1 (Ulk1) Phosphorylates the Co-chaperone Cell Division Cycle Protein 37 (Cdc37) and Thereby Disrupts the Stability of Cdc37 Client Proteins. J. Biol. Chem. 292, 2830–2841. 10.1074/jbc.M116.762443. [PubMed: 28073914]
40. Panaretou B, Prodromou C, Roe SM, O'Brien R, Ladbury JE, Piper PW, and Pearl LH (1998). ATP binding and hydrolysis are essential to the function of the Hsp90 molecular chaperone in vivo. EMBO J. 17, 4829–4836. 10.1093/emboj/17.16.4829. [PubMed: 9707442]
41. Panaretou B, Siligardi G, Meyer P, Maloney A, Sullivan JK, Singh S, Millson SH, Clarke PA, Naaby-Hansen S, Stein R, et al. (2002). Activation of the ATPase activity of hsp90 by the stress-regulated co-chaperone aha1. Mol. Cell. 10, 1307–1318. S1097276502007852 [pii]. [PubMed: 12504007]
42. Meyer P, Prodromou C, Liao C, Hu B, Mark Roe S, Vaughan CK, Vlasic I, Panaretou B, Piper PW, and Pearl LH (2004). Structural basis for recruitment of the ATPase activator Aha1 to the Hsp90 chaperone machinery. EMBO J. 23, 511–519. 10.1038/sj.emboj.7600060.7600060 [pii]. [PubMed: 14739935]
43. Retzlaff M, Hagn F, Mitschke L, Hessling M, Gugel F, Kessler H, Richter K, and Buchner J. (2010). Asymmetric activation of the hsp90 dimer by its co-chaperone aha1. Mol. Cell. 37, 344–354. 10.1016/j.molcel.2010.01.006. [PubMed: 20159554]
44. Mercier R, Wolmarans A, Schubert J, Neuweiler H, Johnson JL, and LaPointe P. (2019). The conserved NxNNWHW motif in Aha-type co-chaperones modulates the kinetics of Hsp90 ATPase stimulation. Nat. Commun. 10, 1273. 10.1038/s41467-019-09299-3. [PubMed: 30894538]
45. Flom GA, Lemieszek M, Fortunato EA, and Johnson JL (2008). Farnesylation of Ydj1 is required for in vivo interaction with Hsp90 client proteins. Mol. Biol. Cell 19, 5249–5258, E08–04-0435 [pii]. 10.1091/mbc.E08-04-0435. [PubMed: 18829866]
46. Louvion JF, Abbas-Terki T, and Picard D. (1998). Hsp90 is required for pheromone signaling in yeast. Mol. Biol. Cell 9, 3071–3083. [PubMed: 9802897]
47. Truman AW, Millson SH, Nuttall JM, King V, Mollapour M, Prodromou C, Pearl LH, and Piper PW (2006). Expressed in the yeast Saccharomyces cerevisiae, human ERK5 is a client of the Hsp90 chaperone that complements loss of the Slt2p (Mpk1p) cell integrity stress-activated protein kinase. Eukaryot. Cell 5, 1914–1924, EC.00263–06 [pii]. 10.1128/EC.00263-06. [PubMed: 16950928]
48. Bresnick EH, Sanchez ER, and Pratt WB (1988). Relationship between glucocorticoid receptor steroid-binding capacity and association of the Mr 90,000 heat shock protein with the unliganded receptor. J. Steroid Biochem. 30, 267–269. [PubMed: 3386251]
49. Fang Y, Fliss AE, Robins DM, and Caplan AJ (1996). Hsp90 regulates androgen receptor hormone binding affinity in vivo. J. Biol. Chem. 271, 28697–28702. [PubMed: 8910505]
50. Binart N, Lombè s M, and Baulieu EE (1995). Distinct functions of the 90 kDa heat-shock protein (hsp90) in oestrogen and mineralocorticosteroid receptor activity: effects of hsp90 deletion mutants. Biochem. J. 311, 797–804. [PubMed: 7487934]

51. Yeh YY, Wrasman K, and Herman PK (2010). Autophosphorylation within the Atg1 activation loop is required for both kinase activity and the induction of autophagy in Saccharomyces cerevisiae. Genetics 185, 871–882. 10.1534/genetics.110.116566. [PubMed: 20439775]
52. Kijanska M, Dohnal I, Reiter W, Kaspar S, Stoffel I, Ammerer G, Kraft C, and Peter M. (2010). Activation of Atg1 kinase in autophagy by regulated phosphorylation. Autophagy 6, 1168–1178. 10.4161/auto.6.8.13849. [PubMed: 20953146]
53. Schopper S, Kahraman A, Leuenberger P, Feng Y, Piazza I, Müller O, Boersema PJ, and Picotti P. (2017). Measuring protein structural changes on a proteome-wide scale using limited proteolysis-coupled mass spectrometry. Nat. Protoc. 12, 2391–2410. 10.1038/nprot.2017.100. [PubMed: 29072706]
54. Paladino A, Woodford MR, Backe SJ, Sager RA, Kancherla P, Daneshvar MA, Chen VZ, Bourboulia D, Ahanin EF, Prodromou C, et al. (2020). Chemical Perturbation of Oncogenic Protein Folding: from the Prediction of Locally Unstable Structures to the Design of Disruptors of Hsp90-Client Interactions. Chemistry 26, 9459–9465. 10.1002/chem.202000615. [PubMed: 32167602]
55. Shintani T, and Klionsky DJ (2004). Cargo proteins facilitate the formation of transport vesicles in the cytoplasm to vacuole targeting pathway. J. Biol. Chem. 279, 29889–29894. 10.1074/jbc.M404399200. [PubMed: 15138258]
56. Kim J, Huang WP, Stromhaug PE, and Klionsky DJ (2002). Convergence of multiple autophagy and cytoplasm to vacuole targeting components to a perivacuolar membrane compartment prior to de novo vesicle formation. J. Biol. Chem. 277, 763–773. 10.1074/jbc.M109134200. [PubMed: 11675395]
57. Suzuki K, Kirisako T, Kamada Y, Mizushima N, Noda T, and Ohsumi Y. (2001). The pre-autophagosomal structure organized by concerted functions of APG genes is essential for autophagosome formation. EMBO J. 20, 5971–5981. 10.1093/emboj/20.21.5971. [PubMed: 11689437]
58. Hawkins WD, and Klionsky DJ (2021). The expanding role of Atg8. Autophagy 17, 3273–3274. 10.1080/15548627.2021.1967566. [PubMed: 34482799]
59. Nair U, Thumm M, Klionsky DJ, and Krick R. (2011). GFP-Atg8 protease protection as a tool to monitor autophagosome biogenesis. Autophagy 7, 1546–1550. 10.4161/auto.7.12.18424. [PubMed: 22108003]
60. Ragusa MJ, Stanley RE, and Hurley JH (2012). Architecture of the Atg17 complex as a scaffold for autophagosome biogenesis. Cell 151, 1501–1512. 10.1016/j.cell.2012.11.028. [PubMed: 23219485]
61. Suzuki K, Kubota Y, Sekito T, and Ohsumi Y. (2007). Hierarchy of Atg proteins in pre-autophagosomal structure organization. Gene Cell. 12, 209–218. 10.1111/j.1365-2443.2007.01050.x.
62. Noda T, Matsuura A, Wada Y, and Ohsumi Y. (1995). Novel system for monitoring autophagy in the yeast Saccharomyces cerevisiae. Biochem. Biophys. Res. Commun. 210, 126–132. 10.1006/bbrc.1995.1636. [PubMed: 7741731]
63. Mizushima N, and Yoshimori T. (2007). How to interpret LC3 immunoblotting. Autophagy 3, 542–545. 10.4161/auto.4600. [PubMed: 17611390]
64. Kabeya Y, Mizushima N, Ueno T, Yamamoto A, Kirisako T, Noda T, Kominami E, Ohsumi Y, and Yoshimori T. (2000). LC3, a mammalian homologue of yeast Apg8p, is localized in autophagosome membranes after processing. EMBO J. 19, 5720–5728. 10.1093/emboj/19.21.5720. [PubMed: 11060023]
65. Hawle P, Siepmann M, Harst A, Siderius M, Reusch HP, and Obermann WMJ (2006). The middle domain of Hsp90 acts as a discriminator between different types of client proteins. Mol. Cell Biol. 26, 8385–8395, MCB.02188–05 [pii]. 10.1128/MCB.02188-05. [PubMed: 16982694]
66. Millson SH, Truman AW, King V, Prodromou C, Pearl LH, and Piper PW (2005). A two-hybrid screen of the yeast proteome for Hsp90 interactors uncovers a novel Hsp90 chaperone requirement in the activity of a stress-activated mitogen-activated protein kinase, Slt2p (Mpk1p). Eukaryot. Cell 4, 849–860, 4/5/849 [pii]. 10.1128/EC.4.5.849-860.2005.

67. Zierer BK, Weiwad M, Rübbelke M, Freiburger L, Fischer G, Lorenz OR, Sattler M, Richter K, and Buchner J. (2014). Artificial accelerators of the molecular chaperone Hsp90 facilitate rate-limiting conformational transitions. Angew. Chem., Int. Ed. Engl. 53, 12257–12262. 10.1002/anie.201406578. [PubMed: 25244159]
68. Woodford MR, Sager RA, Marris E, Dunn DM, Blanden AR, Murphy RL, Rensing N, Shapiro O, Panaretou B, Prodromou C, et al. (2017). Tumor suppressor Tsc1 is a new Hsp90 co-chaperone that facilitates folding of kinase and non-kinase clients. EMBO J. 36, 3650–3665. 10.15252/embj.201796700. [PubMed: 29127155]
69. Barrott JJ, and Haystead TAJ (2013). Hsp90, an unlikely ally in the war on cancer. FEBS J. 280, 1381–1396. 10.1111/febs.12147. [PubMed: 23356585]
70. Wang H, Lu M, Yao M, and Zhu W. (2016). Effects of treatment with an Hsp90 inhibitor in tumors based on 15 phase II clinical trials. Mol. Clin. On-col. 5, 326–334. 10.3892/mco.2016.963.
71. Kurokawa Y, Honma Y, Sawaki A, Naito Y, Iwagami S, Komatsu Y, Takahashi T, Nishida T, and Doi T. (2022). Pimitespib in patients with advanced gastrointestinal stromal tumor (CHAPTER-GIST-301): a randomized, double-blind, placebo-controlled phase III trial. Ann. Oncol. 33, 959–967. 10.1016/j.annonc.2022.05.518. [PubMed: 35688358]
72. Jung CH, Jun CB, Ro SH, Kim YM, Otto NM, Cao J, Kundu M, and Kim DH (2009). ULK-Atg13-FIP200 complexes mediate mTOR signaling to the autophagy machinery. Mol. Biol. Cell 20, 1992–2003. 10.1091/mbc.e08-12-1249. [PubMed: 19225151]
73. Abeliovich H, Zhang C, Dunn WA Jr., Shokat KM, and Klionsky DJ (2003). Chemical genetic analysis of Apg1 reveals a non-kinase role in the induction of autophagy. Mol. Biol. Cell 14, 477–490. 10.1091/mbc.e02-07-0413. [PubMed: 12589048]
74. Kimura S, Noda T, and Yoshimori T. (2007). Dissection of the autophagosome maturation process by a novel reporter protein, tandem fluorescent-tagged LC3. Autophagy 3, 452–460. 10.4161/auto.4451. [PubMed: 17534139]
75. Garabedian MJ, and Yamamoto KR (1992). Genetic dissection of the signaling domain of a mammalian steroid receptor in yeast. Mol. Biol. Cell 3, 1245–1257. [PubMed: 1457829]
76. Schena M, Freedman LP, and Yamamoto KR (1989). Mutations in the glucocorticoid receptor zinc finger region that distinguish interdigitated DNA binding and transcriptional enhancement activities. Genes Dev. 3, 1590–1601. [PubMed: 2515114]
77. Backe SJ, Sager RA, Regan BR, Sit J, Major LA, Bratslavsky G, Woodford MR, Bourboulia D, and Mollapour M. (2022). A specialized Hsp90 co-chaperone network regulates steroid hormone receptor response to ligand. Cell Rep. 40, 111039. 10.1016/j.celrep.2022.111039.
78. Picard D, Khursheed B, Garabedian MJ, Fortin MG, Lindquist S, and Yamamoto KR (1990). Reduced levels of hsp90 compromise steroid receptor action in vivo. Nature 348, 166–168. 10.1038/348166a0. [PubMed: 2234079]
79. Murphy SM, Bergman M, and Morgan DO (1993). Suppression of c-Src activity by C-terminal Src kinase involves the c-Src SH2 and SH3 domains: analysis with Saccharomyces cerevisiae. Mol. Cell Biol. 13, 5290–5300. [PubMed: 7689149]
80. Sager RA, Woodford MR, Backe SJ, Makedon AM, Baker-Williams AJ, DiGregorio BT, Loiselle DR, Haystead TA, Zachara NE, Prodromou C, et al. (2019). Post-translational Regulation of FNIP1 Creates a Rheostat for the Molecular Chaperone Hsp90. Cell Rep. 26, 1344–1356.e5. 10.1016/j.celrep.2019.01.018. [PubMed: 30699359]
81. Oberoi J, Dunn DM, Woodford MR, Mariotti L, Schulman J, Bourboulia D, Mollapour M, and Vaughan CK (2016). Structural and functional basis of protein phosphatase 5 substrate specificity. Proc. Natl. Acad. Sci. USA 113, 9009–9014. 10.1073/pnas.1603059113. [PubMed: 27466404]
82. Schindelin J, Arganda-Carreras I, Frise E, Kaynig V, Longair M, Pietzsch T, Preibisch S, Rueden C, Saalfeld S, Schmid B, et al. (2012). Fiji: an open-source platform for biological-image analysis. Nat. Methods 9, 676–682. 10.1038/nmeth.2019. [PubMed: 22743772]
83. Pettersen EF, Goddard TD, Huang CC, Couch GS, Greenblatt DM, Meng EC, and Ferrin TE (2004). UCSF Chimera–a visualization system for exploratory research and analysis. J. Comput. Chem. 25, 1605–1612. 10.1002/jcc.20084. [PubMed: 15264254]
84. Perez-Riverol Y, Csordas A, Bai J, Bernal-Llinares M, Hewapathir-ana S, Kundu DJ, Inuganti A, Griss J, Mayer G, Eisenacher M, et al. (2019). The PRIDE database and related tools and

resources in 2019: improving support for quantification data. Nucleic Acids Res. 47, D442–D450. 10.1093/nar/gky1106. [PubMed: 30395289]

85. Amberg DC, Burke DJ, and Strathern JN (2006). PCR-Mediated Gene Disruption: One-Step Method. CSH Protoc. 2006, pdb.prot4169. 10.1101/pdb.prot4169.
86. Adams A, Gottschling DE, Kaiser CA, and Stearns T. (1997). Methods in Yeast Genetics (Cold Spring Harbor Laboratory Press).
87. Siligardi G, Hu B, Panaretou B, Piper PW, Pearl LH, and Prodromou C. (2004). Co-chaperone regulation of conformational switching in the Hsp90 ATPase cycle. J. Biol. Chem. 279, 51989–51998, M410562200 [pii]. 10.1074/jbc.M410562200. [PubMed: 15466438]
88. Siligardi G, Panaretou B, Meyer P, Singh S, Woolfson DN, Piper PW, Pearl LH, and Prodromou C. (2002). Regulation of Hsp90 ATPase activity by the co-chaperone Cdc37p/p50cdc37. J. Biol. Chem. 277, 20151–20159. 10.1074/jbc.M201287200M201287200 [pii]. [PubMed: 11916974]
89. Hjorth-Sørensen B, Hoffmann ER, Lissin NM, Sewell AK, and Jakobsen BK (2001). Activation of heat shock transcription factor in yeast is not influenced by the levels of expression of heat shock proteins. Mol. Microbiol. 39, 914–923. mmi2279 [pii]. [PubMed: 11251812]
90. Kim S, Backe SJ, Wengert LA, Johnson AE, Isakov RV, Bratslavsky MS, and Woodford MR (2022). O-GlcNAcylation suppresses TRAP1 activity and promotes mitochondrial respiration. Cell Stress Chaperones 27, 573–585. 10.1007/s12192-022-01293-x. [PubMed: 35976490]
91. Woodford MR, Baker-Williams AJ, Sager RA, Backe SJ, Blanden AR, Hashmi F, Kancherla P, Gori A, Loiselle DR, Castelli M, et al. (2021). The tumor suppressor folliculin inhibits lactate dehydrogenase A and regulates the Warburg effect. Nat. Struct. Mol. Biol. 28, 662–670. 10.1038/s41594-021-00633-2. [PubMed: 34381247]

Highlights

- Autophagy-initiating kinase Atg1/Ulk1 phosphorylates a conserved serine in Hsp90
- Atg1/Ulk1-mediated phosphorylation of Hsp90 is essential for autophagy induction
- Hsp90 phosphorylation by Atg1/Ulk1 regulates client protein activity
- Phosphorylation of Hsp90 is essential for Atg1 conformational change and activity

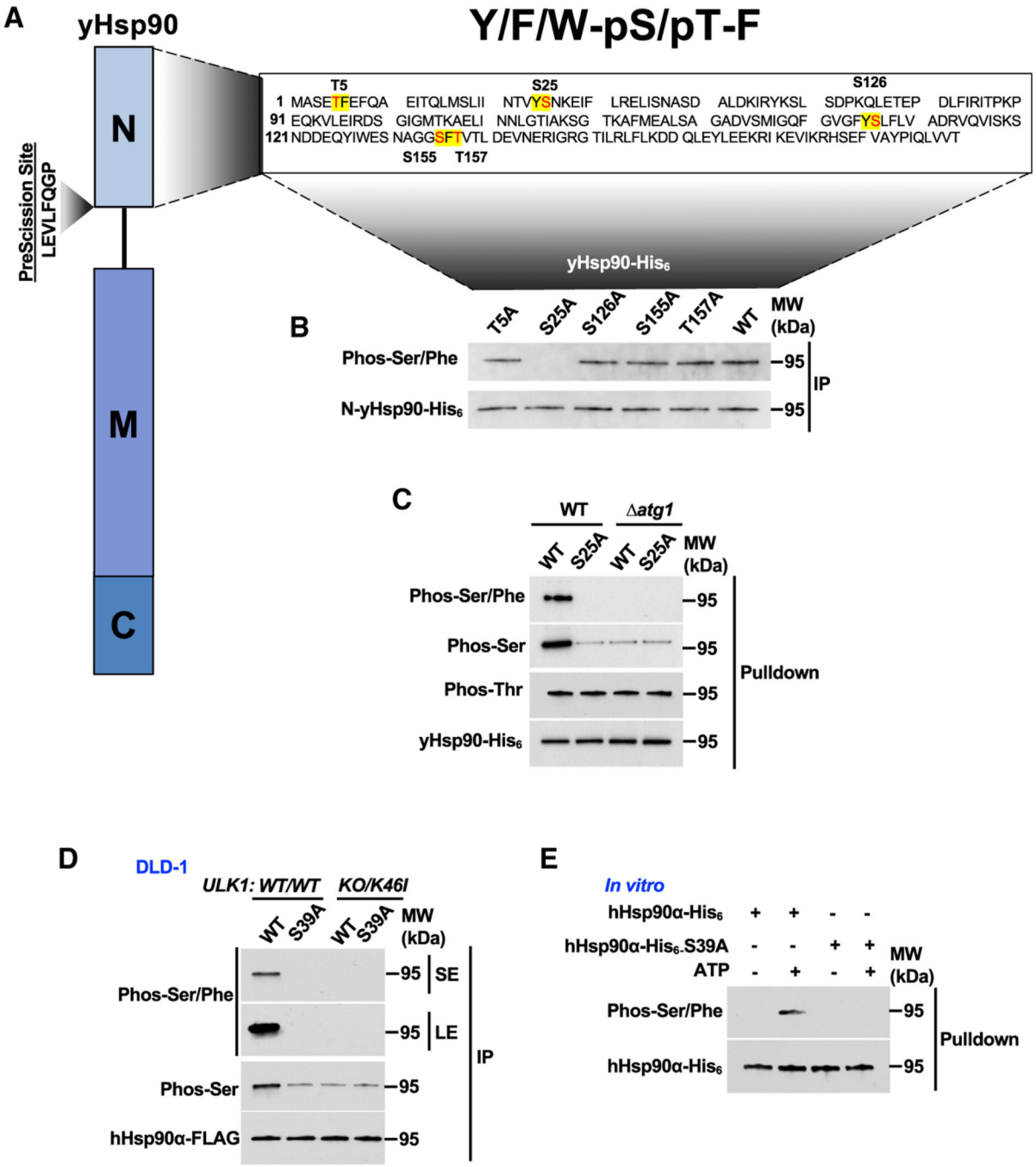

Figure 1. Ulk1-mediated phosphorylation of a conserved serine in amino domain of Hsp90

(A) Schematic representation of yHsp90 domain architecture. A PreScission Protease cleavage motif was inserted between the N-terminal domain and the charged linker. Amino acid residues within the yHsp90 N-terminal domain fitting the consensus phosphorylated (phos)-(Ser/Thr) Phe motif are colored red, with the surrounding motif highlighted yellow. (B) WT-yHsp90-His_6 or indicated yHsp90 mutants were expressed as the sole copy of Hsp90 in yeast. yHsp90-His_6 was isolated by Ni-NTA pulldown. The N-domain was further

isolated by cleavage with PreScission Protease, and phosphorylation of N-yHsp90-His_6 was determined by immunoblotting with an anti-Phos-(Ser/Thr) Phe antibody.

(C) yHsp90-His_6-WT or S25A was expressed in yeast with *ATG1* expressed (WT) or *ATG1* knocked out (Δ*atg1*). yHsp90-His_6 was isolated by Ni-NTA pull-down, and phosphorylation was evaluated by immunoblotting with antibodies against phos-Thr, phos-Ser, or phos-(Ser/Thr) Phe.

(D) DLD-1 cells stably expressing WT *ULK1* or kinase-dead *ULK1* (K46I) were transiently transfected with hHsp90α-FLAG-WT or S39A. hHsp90-FLAG was isolated by immunoprecipitation (IP), and levels of phos-(Ser/Thr) Phe and phos-Ser were determined by western blot.

(E) Recombinant hHsp90alpha-WT or S39A was incubated with Ulk1 and with or without ATP. hHsp90alpha was isolated by Ni-NTS pulldown, and levels of phos-(Ser/Thr) Phe were determined by immunoblot.

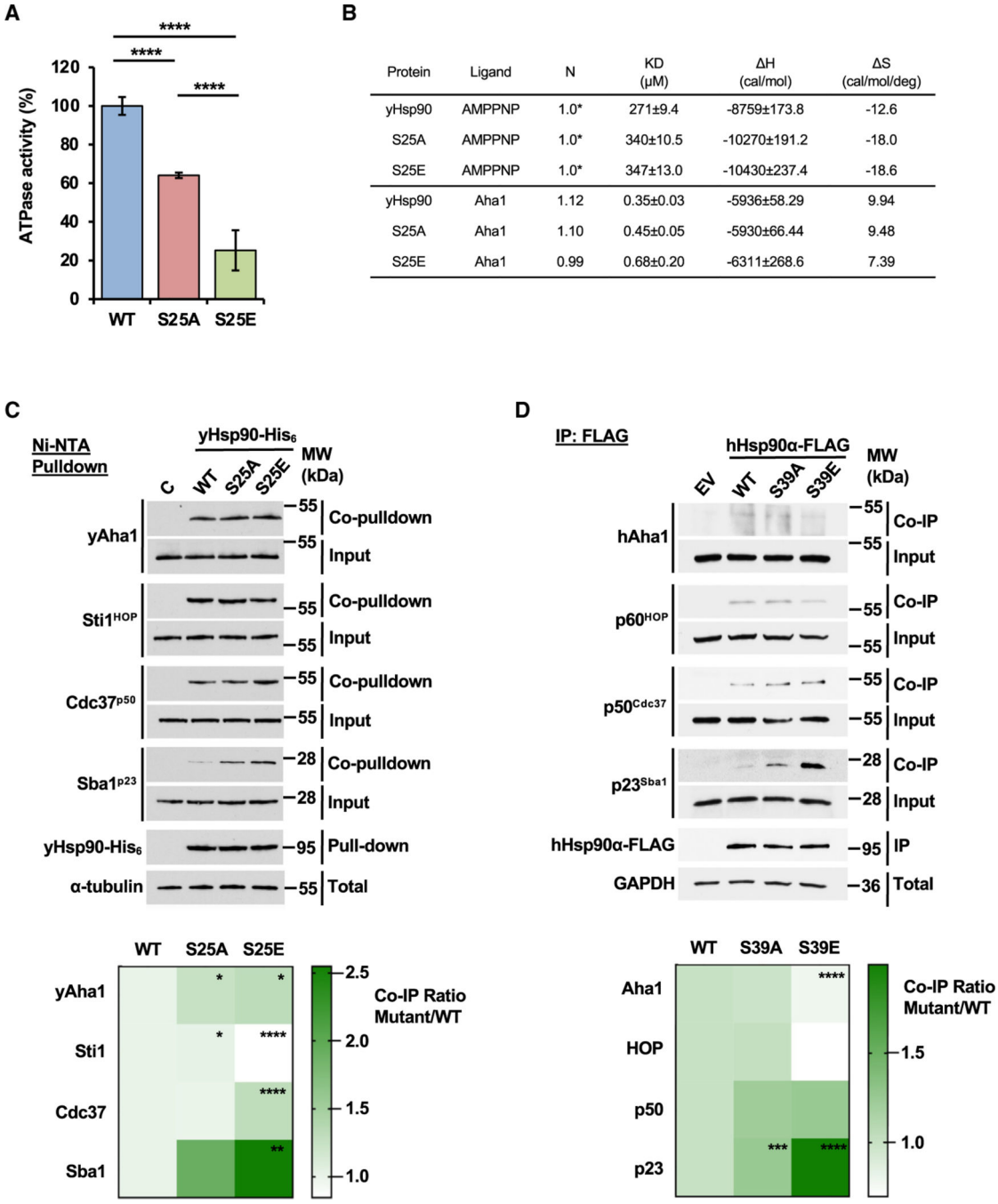

Protein	Ligand	N	KD (μM)	ΔH (cal/mol)	ΔS (cal/mol/deg)
yHsp90	AMPPNP	1.0*	271±9.4	-8759±173.8	-12.6
S25A	AMPPNP	1.0*	340±10.5	-10270±191.2	-18.0
S25E	AMPPNP	1.0*	347±13.0	-10430±237.4	-18.6
yHsp90	Aha1	1.12	0.35±0.03	-5936±58.29	9.94
S25A	Aha1	1.10	0.45±0.05	-5930±66.44	9.48
S25E	Aha1	0.99	0.68±0.20	-6311±268.6	7.39

Figure 2. Phosphorylation of S25/S39 affects Hsp90 ATPase activity and co-chaperone binding

(A) yHsp90-WT, S25A, and S25E were bacterially expressed and purified and used in an ATPase assay. ATP hydrolysis rates are presented as a parentage of the rate of WT-yHsp90. Data represent the mean and standard deviation of 3 independent replicates. A Student's t test was used to determine significance (****$p < 0.0001$).

(B) ITC was used to determine the affinity of WT-yHsp90, S25A, and S25E for ligand (AMPPNP) and the co-chaperone Aha1. N, stoichiometry of the interaction; knockdown (KD) (μM), dissociation constant; ΔH (cal/mol), enthalpy; ΔS (cal/mol/°), entropy.

(C) Lysate was collected from yeast expressing WT-yHsp90-His_6, S25A, or S25E as the sole copy of Hsp90. Ni-NTA pull-down was performed to isolate yHsp90-His_6. Co-pull-down of co-chaperones was evaluated by western blot. PP30-Ycplac195-*Hsc82* was used as a control (C). α-Tubulin was used as a loading control. Densitometry was performed using ImageStudioLite v.5.2.5 to quantify western blot band signal intensity. Heatmap colors represent the mean signal intensity values of co-chaperone coIP normalized to WT. Tukey's multiple comparisons test was used to determine statistical significance for three independent measurements. *$p < 0.05$, **$p < 0.01$, ***$p < 0.001$, and ****$p < 0.0001$. (D) HEK293 cells were transiently transfected with hHsp90α-FLAG-WT, S39A, S39E, or empty vector (EV) as a control. hHsp90α-FLAG was isolated by IP, and coIP of co-chaperones was determined by western blot. GAPDH was used as a loading control. Densitometry was performed using ImageStudioLite v.5.2.5 to quantify western blot band signal intensity. Heatmap colors represent the mean signal intensity values of co-chaperone coIP normalized to WT. Tukey's multiple comparisons test was used to determine statistical significance for three independent measurements. *$p < 0.05$, **$p < 0.01$, ***$p < 0.001$, and ****$p < 0.0001$.

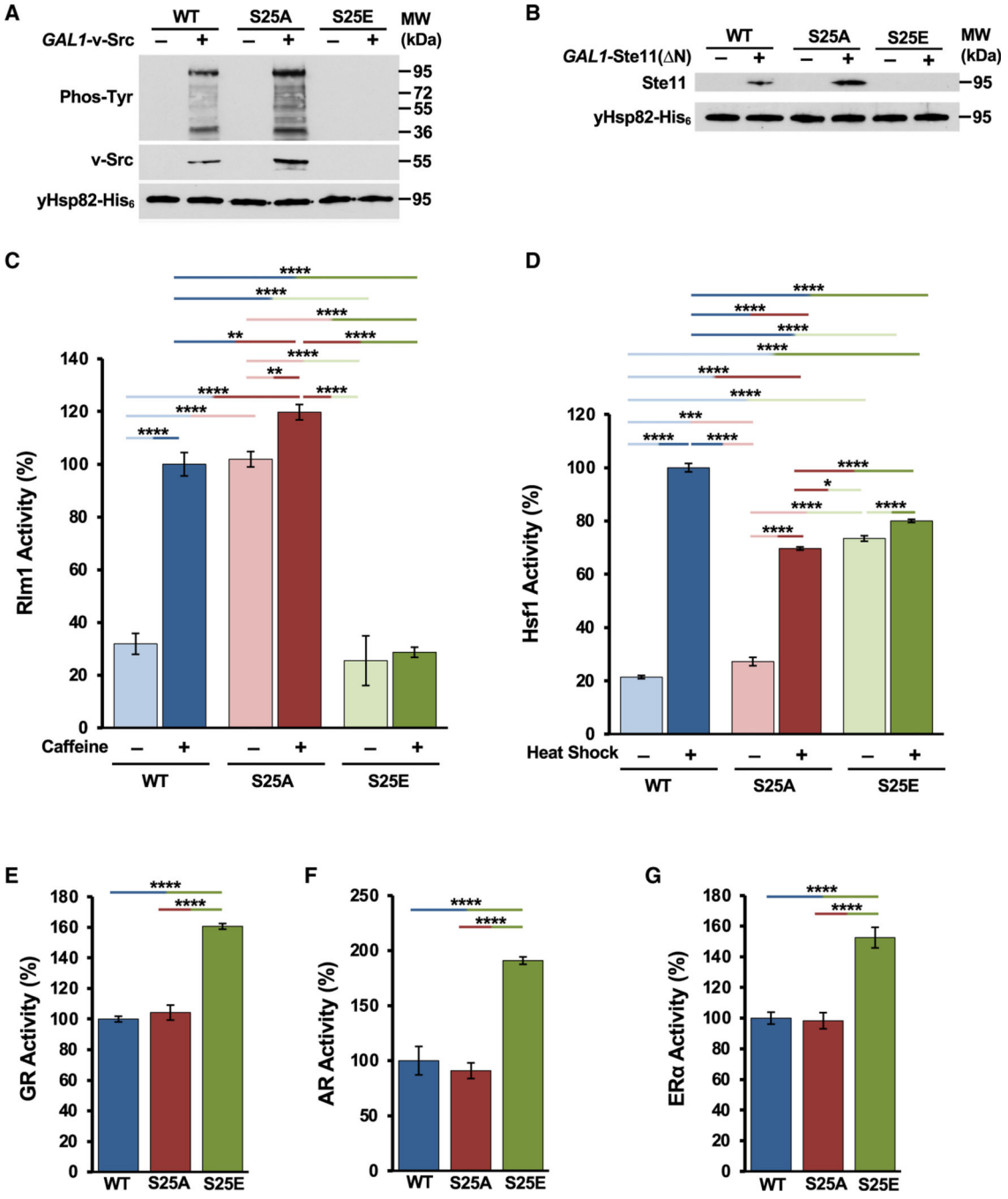

Figure 3. yHsp90-S25 phosphomutants impact chaperoning of client proteins

(A) *GAL1-v-SRC* was transformed into yeast cells expressing yHsp90-His_6-WT, S25A, or S25E. Yeast was grown on glucose (−) or galactose (+) to induce v-Src expression. v-Src stability was determined by western blot for total v-Src protein. v-Src activity was determined by western blotting with an anti-pan-phosphotyrosine antibody.

(B) Yeast with yHsp90-His_6-WT, S25A, or S25E was also transformed with *GAL1-Ste11(ΔN)-myc*. Cells were grown on glucose (−) or galactose (+) media, and Ste11(ΔN)-myc protein stability was examined by immunoblotting.

(C) *RLM1-LacZ* reporter plasmid was transformed into yeast expressing yHsp90-His_6-WT, S25A, or S25E. Cells were grown to mid-log phase and stressed with 8 mM caffeine for 4 h. Rlm1 activity was measured using a β-galactosidase assay. Data are presented as mean ± standard deviation derived from three inde pendent replicates. Tukey's multiple comparisons test was used to determine statistical significance. **p < 0.01, ***p < 0.001, and ****p < 0.0001.

(D) Yeast with yHsp90-His_6-WT, S25A, or S25E was also transformed with *HSE-LacZ* reporter plasmid. Hsf1 activity was measured by β-galactosidase assay after cells were heat shocked at 39°C for 40 min. Data are presented as mean ± standard deviation derived from three independent replicates. Tukey's multiple comparisons test was used to determine statistical significance. *p < 0.05, **p < 0.01, ***p < 0.001, and ****p < 0.0001.

(E) Yeast expressing yHsp90-His_6-WT, S25A, or S25E was transformed with GR and *GRE-LacZ* reporter plasmids. Cells were grown to mid-log phase followed by the addition of 30 μM dexamethasone for 2.5 h. GR activity was measured by β-galactosidase assay. Data are presented as mean ± standard deviation derived from three independent replicates. Tukey's multiple comparisons test was used to determine statistical significance. ****p < 0.0001.

(F) Yeast expressing yHsp90-His_6-WT, S25A, or S25E was transformed with AR and *GRE-LacZ* reporter plasmids. Cells were grown to mid-log phase followed by the addition of 20 nM dihydrotestosterone (DHT) for 2.5 h. AR activity was measured by β-galactosidase assay. Data are presented as mean ± standard deviation derived from three independent replicates. Tukey's multiple comparisons test was used to determine statistical significance. ****p < 0.0001.

(G) Yeast expressing yHsp90-His_6-WT, S25A, or S25E was transformed with ERα and *ERE-LacZ* reporter plasmid. Cells were grown to mid-log phase followed by the addition of 200 nM β-estradiol for 2.5 h. ERa activity was measured by β-galactosidase assay. Data are presented as mean ± standard deviation derived from three independent replicates. Tukey's multiple comparisons test was used to determine statistical significance. ****p < 0.0001.

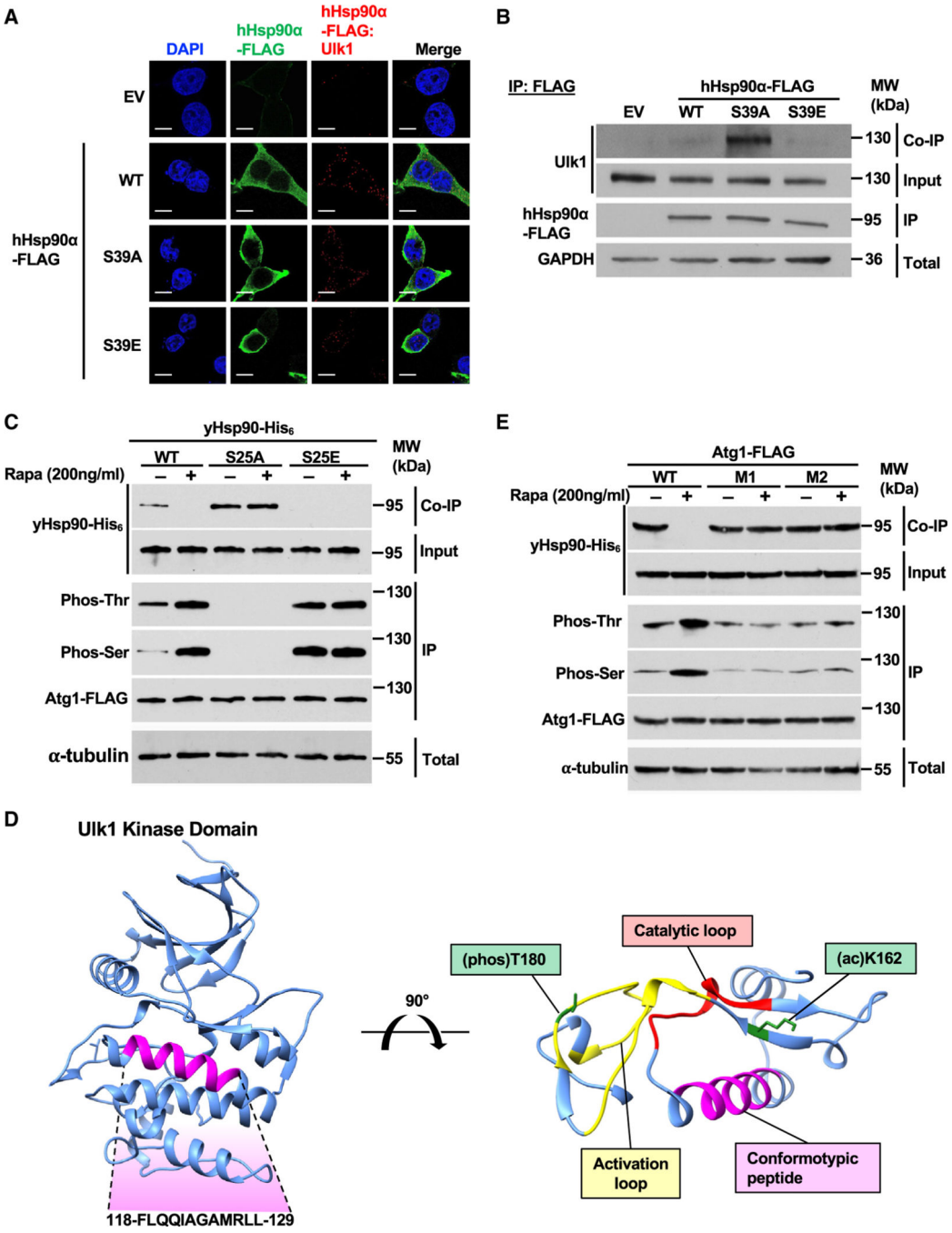

Figure 4. Phosphorylation of S25-Hsp90 is essential for Atg1/Ulk1 activity

(A) HEK293 cells were transfected with hHsp90α-FLAG-WT, S39A, S39E, or EV as a control. Immunofluorescence staining was used to detect total hHsp90α-FLAG protein (green). Duolink proximity ligation assay was used to detect hHsp90α-FLAG:Ulk1 complexes (red). DAPI was used for nuclear staining. Scale bar is 10 μm.

(B) hHsp90α-FLAG-WT, S39A, or S39E was transiently expressed and isolated from HEK293 cells. coIP of endogenous Ulk1 was evaluated by immunoblot. EV was used as a control. GAPDH was used as a loading control.

(C) Yeast expressing yHsp90-His_6-WT, S25A, or S25E in the Δ*atg1* strain was transformed with Atg1-FLAG. Cells were grown to mid-log phase and left untreated (−) or treated with 200 ng/mL rapamycin (+) for 20 min. Atg1-FLAG was isolated by IP, and Atg1 phosphorylation was evaluated by immunoblot for phos-Ser and phos-Thr. coIP of yHsp90-His was determined by immunoblot. α-Tubulin was used as a loading control.
(D) LiP-MS was performed on Ulk1:hHsp90α and Ulk1:hHsp90α+ATP to identify regions of altered protease sensitivity. Ribbon structure of the Ulk1 kinase domain (AlphaFold-O75385) with the conformotypic peptide (F118-L129) is highlighted magenta (left). The proximity of the conformotypic peptide to functionally important regions of Ulk1 was visualized using Chimera Chimera v.1.14 (UCSF). Conformotypic peptide: magenta; activation loop: yellow; catalytic loop: red; PTM (phos-T180, acK162): green.
(E) Yeast expressing yHsp90-His_6-WT in the Δ*atg1* strain was transformed with Atg1-FLAG-WT or conformotypic peptide mutants. Cells were grown to mid-log phase and left untreated (−) or treated with 200 ng/mL rapamycin (+) for 20 min. Atg1-FLAG was isolated by IP, and Atg1 phosphorylation was evaluated by immunoblot for phos-Ser and phos-Thr. coIP of yHsp90-His was determined by immunoblot. α-Tubulin was used as a loading control.

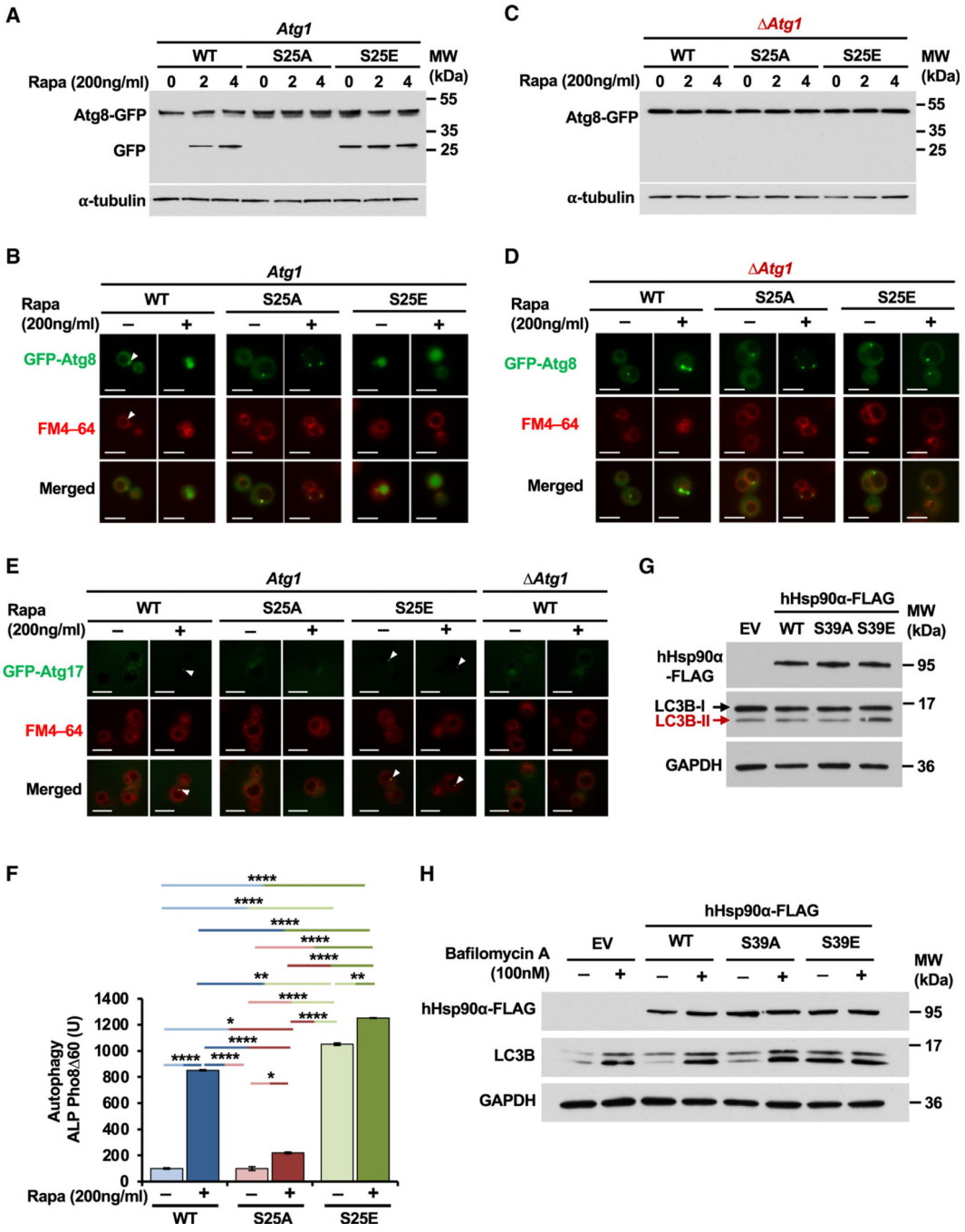

Figure 5. Atg1/Ulk1-mediated phosphorylation of Hsp90 is essential for autophagy induction

(A) Yeast expressing yHsp90-His_6-WT, S25A, or S25E was transformed with GFP-Atg8. Cells were grown to mid-log phase and treated with rapamycin (200 ng/mL) for the indicated times. Induction of autophagy was evaluated by immunoblotting for GFP to detect cleavage of Atg8. α-Tubulin was used as loading control.

(B) Yeast expressing yHsp90-His_6-WT, S25A, or S25E and GFP-Atg8 was grown to mid-log phase and treated with rapamycin (200 ng/mL) for 2 h. Cells were stained with 8 mM

vacuole marker FM4–64 (red) for 30 min prior to imaging. Induction of autophagy was evaluated by visualizing localization of GFP-Atg8 to the vacuole. Scale bar is 5 μm.
(C) *ATG1* was knocked out of yeast expressing yHsp90-His_6-WT, S25A, or S25E and GFP-Atg8. Cells were grown to mid-log phase and treated with rapamycin (200 ng/mL) for the indicated times. Induction of autophagy was evaluated by immunoblotting for GFP to detect cleavage of Atg8. α-Tubulin was used as loading control.
(D) Yeast with *ATG1* KO expressing yHsp90-His_6-WT, S25A, or S25E and GFP-Atg8 was treated with rapamycin (200 ng/mL) for 2 h. Cells were stained with 8 mM vacuole marker FM4–64 (red) for 30 min prior to imaging. Induction of autophagy was evaluated by visualizing localization of GFP-Atg8 to the vacuole. Scale bar is 5 μm.
(E) Yeast expressing yHsp90-His_6-WT, S25A, or S25E and GFP-Atg17 was grown to mid-log phase and treated with rapamycin (200 ng/mL) for 2 h. Yeast with *ATG1* KO expressing yHsp90-His_6-WT was used as a control. Cells were stained with 8 mM vacuole marker FM4–64 (red) for 30 min prior to imaging. Pre-autophagosomal structure formation was evaluated by visualizing localization of GFP-Atg17 to the vacuole. Scale bar is 5 μm.
(F) Pho8Δ60 gene was transformed into yeast expressing yHsp90-His_6-WT or the phosphomutant S25A or S25E. Cells were grown to mid-log phase and left untreated (−) or treated with 200 ng/mL rapamycin (rapa) for 4 h. ALP activity is presented as emission per the amount of protein in the reaction (mg) and the reaction time (mins). Data are presented as mean ± standard deviation derived from three independent replicates. Tukey's multiple comparisons test was used to determine statistical significance. *$p < 0.05$, **$p < 0.01$, ***$p < 0.001$, and ****$p < 0.0001$.
(G) HEK293 cells were transfected with hHsp90α-FLAG-WT, S39A, S39E, or EV as a control. Induction of autophagy was determined by immunoblotting for LC3B. GAPDH was used as a loading control.
(H) HEK293 cells transiently expressing hHsp90α-FLAG-WT, S39A, S39E, or EV was treated with Bafilomycin A (100 nM) for 16 h. Induction of autophagy was determined by immunoblotting for LC3B. GAPDH was used as a loading control.

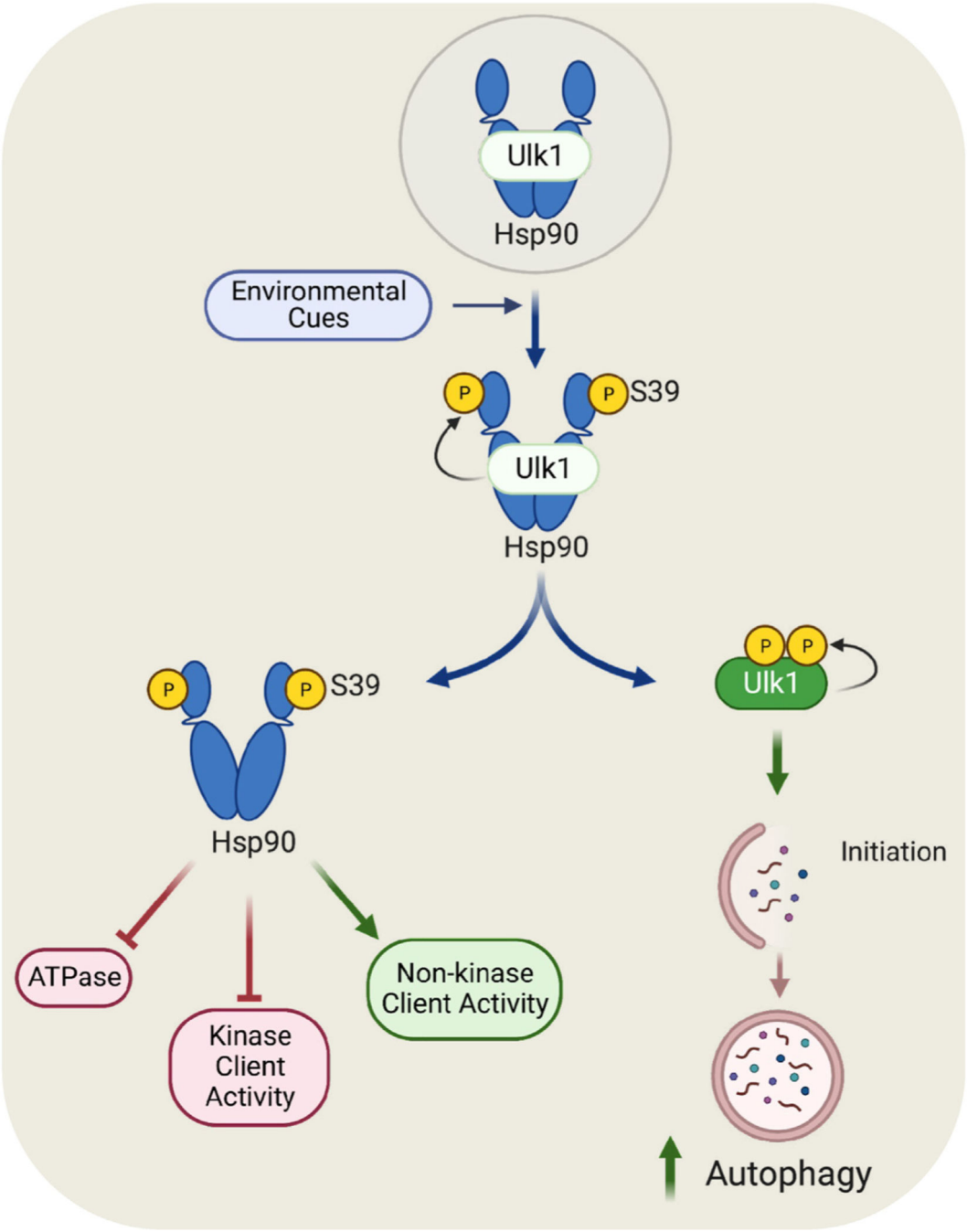

Figure 6. Atg1/Ulk1-mediated phosphorylation of Hsp90 regulates chaperone function and promotes induction of autophagy

Schematic model of Ulk1:Hsp90-mediated regulation of autophagy. Hsp90 chaperones Ulk1 and holds the kinase in an inactive state. Environmental cues trigger Ulk1 to phosphorylate hHsp90α-S39, which inhibits Hsp90 ATPase activity and the chaperoning of kinase clients but promotes non-kinase client activity. Conversely, Hsp90 phosphorylation leads to dissociation of Ulk1, allowing for Ulk1 autophosphorylation and subsequent activity. The culmination of these events results in increased cellular autophagic flux.

KEY RESOURCES TABLE

REAGENT or RESOURCE	SOURCE	IDENTIFIER
Antibodies		
Rabbit anti-FLAG tag	Thermo Scientific	Cat# PA1–984B; RRID:AB_347227
Mouse anti-6x-His epitope tag (HIS.H8)	Thermo Scientific	Cat# MA1–21315; RRID:AB_557403
Rabbit anti-p23	Enzo Life Sciences	Cat# ADI-SPA-670-D; RRID:AB_991602
Rabbit anti-Cdc37	StressMarq Biosciences	Cat# SPC-142; RRID:AB_2570605
Rabbit anti-Aha1	StressMarq Biosciences	Cat# SPC-183; RRID:AB_1944037
Rabbit anti-GR (D6H2L)	Cell Signaling Technology	Cat# 12041; RRID:AB_2631286
Rabbit anti-AR (D6F11)	Cell Signaling Technology	Cat# 5153; RRID:AB_10691711
Rabbit anti-ERα (D6R2W)	Cell Signaling Technology	Cat# 13258; RRID:AB_2632959
Rabbit anti-myc tag (71D10)	Cell Signaling Technology	Cat# 2278; RRID:AB_490778
Rabbit anti-HOP	Cell Signaling Technology	Catt# 5670; RRID:AB_10828378
Rabbit anti-Cdc37	Cell Signaling Technology	Catt# 4793; RRID:AB_10695539
Rabbit anti-Ulk1	Cell Signaling Technology	Catt# 8054; RRID:AB_11178668
Rabbit anti-LC3B	Cell Signaling Technology	Catt# 3868; RRID:AB_2137707
Mouse anti-GAPDH	Cell Signaling Technology	Cat# 97166; RRID:AB_2756824
Rabbit anti-phospho-(Ser/Thr)Phe	Cell Signaling Technology	Cat# 9631; RRID:AB_330308
Mouse anti-phospho-threonine (PTR-8)	Sigma-Aldrich	Cat# P6623; RRID:AB_477393
Mouse anti-phospho-serine (PSR-45)	Sigma-Aldrich	Cat# P5747; RRID:AB_477376
Mouse anti-GFP	Biolegend	Cat# B34 902601; RRID:AB_2565021
Rat anti-tubulin	Abcam	Cat# ab6161; RRID:AB_305329
Mouse anti-phospho-tyrosine (4G10)	Millipore	Cat# 05–321; RRID:AB_309678
Mouse anti-v-src (clone 327)	Millipore	Cat# MABS193; RRID:AB_11205595
anit-Stil^{HOP}	Dr. Daniel C. Masson, National Cancer Institute, USA	N/A
anit-Sbal^{p23}	Institute of Cancer Research, UK	N/A
anit-Cdc37^{p50}	Dr. Len Neckers, National Cancer Institute, USA	N/A
anit-yAhal	Dr. Len Neckers, National Cancer Institute, USA	N/A
Anti-mouse Alexa Fluor secondary	ThermoFisher Scientific	Cat# A-11001; RRID:AB_2534069
Anti-mouse secondary	Cell Signaling Technology	Cat# 7076; RRID:AB_330924
Anti-rabbit secondary	Cell Signaling Technology	Cat# 7074; RRID:AB_2099233
Anti-rat secondary	Cell Signaling Technology	Cat# 7077; RRID:AB_10694715
Bacterial and virus strains		
BL21(DE3)	ThermoFisher Scientific	Cat# EC0114
DH5-alpha Electrocompetent E coli	GoldBio	Cat# CC-203
Chemicals, peptides, and recombinant proteins		
ATP	Sigma-Aldrich	Cat# FLAAS
ATP	Sigma-Aldrich	Cat# A9187

REAGENT or RESOURCE	SOURCE	IDENTIFIER
Phosphoenol pyruvate	Roche	Cat# 10108294
Pyruvate kinase	Roche	Cat# 10109045001
Lactate Dehydrogenase	Sigma-Aldrich	Cat# L1006
NADH	Roche	Cat# 10128023001
Recombinant Hsp90α	Dr. Chrisostomos Prodromou, University of Sussex	N/A
Ulk1	Abcam	Cat# ab95322
PreScission Protease	GenScript	Cat# Z02799
TPCK-Trypsin	Sigma-Aldrich	Cat# T1426
FM4–64	ThermoFisher Scientific	Cat# T13320
Rapamycin	LC Laboratories	Cat# R-5000
Biotin-Ganetespib	Synta Pharmaceuticals	Cat# STA-12–7346
Caffeine	Millipore-Sigma	Cat# C0750–500G
Dexamethasone	Millipore-Sigma	Cat# D4902
DHT	Millipore-Sigma	Cat# D-073
β-Estradiol	Millipore-Sigma	Cat# E2758
Nourseothricin	Gold Biotechnology	Cat# N-500–100
Alpha-napthyl phosphate disodium salt	Sigma-Aldrich	Cat# N7255
Bafilomycin A1	LC Laboratories	Cat# B-1080
Critical commercial assays		
Mirus TransIT-2020	MirusBio	Cat# MIR5405
Anti-FLAG M2 affinity gel	Sigma-Aldrich	Cat# A2220
Duolink Proximity Ligation Assay	Millipore-Sigma	Cat# DUO92101
Ni-NTA Agarose	ThermoFisher Scientific	Cat# 88221
ATP agarose	Novus Biologicals	Cat# 510–0002
Strept agarose	ThermoFisher Scientific	Cat# 20349
Deposited data		
Raw and analyzed data	This paper	ProteomeXchange Consortium via the PRIDE; PDX038924
Experimental models: Cell lines		
HEK293	ATCC	Cat# CRL-1573; RRID:CVCL_0045
HAP1 WT	Horizon Discovery	Cat# C631; RRID:CVCL_Y019
HAP1 Ulk1 KO	Horizon Discovery	Cat# HZGHC000072c011; RRID:CVCL_TW31
DLD-1 WT	Horizon Discovery	Cat# HD PAR-111; RRID:CVCL_0248
DLD-1 Ulk1 (K46I/+cKO)	Horizon Discovery	Cat# HD 105–025
Experimental models: Organisms/strains		
PP30-*HSP82*-His_6	Mollapour et al.[4]	N/A
Oligonucleotides		

REAGENT or RESOURCE	SOURCE	IDENTIFIER
DNA primers	Eurofins Genomics	See Table S1
Recombinant DNA		
pRS416-ATG1-FLAG	This study	N/A
pHsp82-His_6-Presc	Mollapour et al. and Mollapour et al.[37,38]	N/A
pRK-Ulk1-myc	Jung et al.[72]	Cat# 31961; RRID:Addgene_31961
GFP-ATG8	Abeliovich et al.[73]	Cat# 49425; RRID:Addgene_49425
pJK59-ATG17-GFP	Ragusa et al.[60]	Cat# 44175; RRID:Addgene_44175
ptfLC3	Kimura et al.[74]	Cat# 21074; RRID:Addgene_21074
pHCA/rGR	Garabedian and Yamamoto[75]	N/A
GRE-LacZ	Schena et al.[76]	N/A
AR	Backe et al.[77]	N/A
ER	Backe et al.[77]	N/A
pUCdeltaSS-ERE	Picard et al.[78]	N/A
2xRLM1-LacZ	Truman et al.[47]	N/A
4XHSE-*LacZ*-pUp41a	Truman et al.[47]	N/A
YpRS426-*GAL 1-v-Src*	Murphy et al.[79]	N/A
STE11 ΔN-myc-pYES2	Sager et al.[80]	N/A
pcDNA3-Cdc37-FLAG WT	Oberoi et al.[81]	N/A
pRSETA-Hsp82-His_6	Panaretou et al.[40]	N/A
Software and algorithms		
Biorender	https://biorender.com/	N/A
Fiji (ImageJ)	Schindelin et al.[82]	https://ImageJ.net/software/fiji/
UCSF Chimera, candidate version 1.14	Pettersen et al.[83]	https://www.cgl.ucsf.edu/chimera/
GraphPad Prism version 9.2.0 for macOS		GraphPad Software, La Jolla, California, USA, www.graphpad.com